ELSEVIER

Contents lists available at ScienceDirect

# International Journal of Pharmaceutics

journal homepage: www.elsevier.com/locate/ijpharm





# Impact of altered hydrophobicity and reduced agglomeration on dissolution of micronized poorly water-soluble drug powders after dry coating

Sangah Kim, Ecevit Bilgili, Rajesh N. Davé

New Jersey Center for Engineered Particulates, New Jersey Institute of Technology, Newark, NJ 07102, USA

#### ARTICLE INFO

Keywords:
Dry coating
Agglomeration
Wettability
Hydrophobicity
Contact angle
Dissolution
BCS Class II drugs

#### ABSTRACT

The impact of dry coating with hydrophobic or hydrophilic nano-silica at 25–100% surface area coverage on dissolution of micronized poorly water-soluble drugs was investigated by examining their agglomeration and surface hydrophobicity. Ibuprofen (20  $\mu m$  and 10  $\mu m$ ) and griseofulvin (10  $\mu m$ ) were selected having differing solubility, hydrophobicity, and surface morphology. Characterization involved particle agglomeration via two dry dispersion methods, drug dissolution using the USP IV method, cohesion reduction through shear testing, and powder wettability via the modified Washburn method. Dry coating dramatically reduced the cohesion hence agglomerate size of both the coated ibuprofen particles, but less for griseofulvin, attributed to its surface morphology. For hydrophobic silica, agglomerate size reduction outweighed the adverse impact of increased surface hydrophobicity for ibuprofen. For griseofulvin, the agglomerate reduction was much lower, not able to overcome the effect of increased drug particle hydrophobicity with hydrophobic silica coating. Hydrophilic silica coating reduced hydrophobicity for all three drug powders, leading to the synergistic improvement in the dissolution along with agglomerate size reduction. Overall, the combined effect of the drug particle surface hydrophobicity and agglomerate size, represented by specific surface area, could explain the dissolution behavior of these poorly water-soluble drugs.

# 1. Introduction

Dry particle coating, where smaller guest particles are attached on larger host particle surfaces, is increasingly popular for altering the surface properties and/or functionality of particles (Chen et al. 2018a; Chen et al. 2008; Naito et al. 2003; Pfeffer et al. 2001; Yang et al. 2005; Yokoyama et al. 1987). Being an environmentally benign solvent-less process, it has been applied to wide varieties of materials in various applications. Among those, increase in powder flow after coating with very small amounts of nano-silica (Chen et al. 2018a; Chen et al. 2008; Naito et al. 2003; Han et al. 2013a; Jallo et al. 2012; Pfeffer et al. 2001; Yang et al. 2005; Yokoyama et al. 1987), improvement in packed bed porosity (Capece et al. 2014), and enhanced fluidization of fine particles (Chen et al. 2008) are some of the interesting implementations. In addition, industrial applicability of dry coating has been demonstrated through utilizing commercial devices such as the conical mill, called comil, including model-supported understanding of comil operating parameters and demonstrating the performance comparability between various devices (Chen et al. 2018b; Chen et al. 2020; Deng et al. 2015; Huang et al. 2015a; Mullarney et al. 2011). Recent pharmaceutical applications have demonstrated the impact of dry coating on enhanced tablet properties (Huang et al. 2015b; Kunnath et al. 2018), enhanced dissolution for hydrophilic silica coated ibuprofen (Han et al. 2013a; Han et al. 2011), and reduced agglomeration of micronized acetaminophen after dry coating hydrophobic silica on improving the content uniformity of blends (Huang et al. 2017). Nonetheless, the synergistic effect that dry coating can bring in terms of reduced agglomeration, as well as changed surface wettability on drug dissolution, remains underexplored, especially for poorly water-soluble drugs.

There are a few notable examples of work demonstrating the influence of hydrophilic or hydrophobic coating materials (Han et al. 2013a; Han et al. 2011; Llusa et al. 2010; Osorio and Muzzio 2015; Pingali et al. 2011a; Pingali et al. 2011b; Qu et al. 2015; Swaminathan et al. 2006). For example, an increase in the dissolution rate of micronized ibuprofen ( $d_{50}$  of 20  $\mu$ m) after dry coating with hydrophilic silica was demonstrated in powder form as well as in tablets formulated with high drug content (Han et al. 2013a; Han et al. 2011). However, the surface hydrophobicity effect after dry coating was not examined. The lubricant

E-mail address: dave@njit.edu (R.N. Davé).

<sup>\*</sup> Corresponding author at: Chemical and Materials Engineering, New Jersey Center for Engineered Particulates New Jersey Institute of Technology, Newark, NJ 07102, USA.

material such as magnesium stearate (MgSt) has been shown to coat the surface of microcrystalline cellulose (MCC) powders during blending as the total strain and shear increased (Swaminathan et al. 2006). Such coating decreased the dispersive surface energy of the blend, attributed to coverage of some of the MCC high-energy sites by MgSt. In other reports, lubrication with MgSt was found to increase the hydrophobicity of the lubricant blend with excipient (Llusa et al. 2010) as well as with acetaminophen, a water-soluble drug (Pingali et al. 2011a). Over lubrication of MgSt was also shown to slow down the dissolution of the drug from tablets (Pingali et al. 2011b). Thus, the consensus has been that lubrication with MgSt leads to weaker tablets, attributed to reduced dispersive surface energy, and slows down drug dissolution due to increased hydrophobicity. Interestingly, a recent work reported (Qu et al. 2015) an increase in the dissolution rate of as received ibuprofen  $(d_{50} \text{ of } 25 \mu\text{m})$  when the drug powder was dry coated with either hydrophobic silica or MgSt, although the powder hydrophobicity was not reported. Such counterintuitive results were likely because of the reduced cohesion and better dispersion of drug powders after dry coating despite coating with hydrophobic materials. Although the extent of powder agglomeration before and after dry coating was not reported, dry coating could have led to reduced agglomeration, which in part could lead to higher dissolution rate. All these results lead to an important question; what is the net effect of dry coating on the dissolution of poorly-soluble drugs? The answer is not obvious because of two competing and confounding effects, namely, the change in surface hydrophobicity (or wettability) and reduced agglomeration. This work investigates this interesting problem by considering two poorly watersoluble, hydrophobic drugs, and both hydrophilic and hydrophobic silica as coating materials.

The topic of the reduced agglomeration of drug particles upon dry coating has not been well-explored. There are a few reports that implicitly discussed the reduced agglomeration by examining the effect on dissolution of drugs as powders and in tablets, and one explicit report that demonstrated reduced agglomeration enabling better drug content uniformity in blends (de Villers 1996, Han et al. 2013a; Han et al. 2011; Huang et al. 2017; Kunnath et al. 2018). Unfortunately, such studies cannot provide assessments of the dynamic nature of the state of powder agglomeration, which is not only a function of external stresses in the blend but is also affected by the nature of sample preparation. This study will examine how dry coating materials affect the drug agglomerate size as well as hydrophobicity of coated drug powders, and how those relate to their dissolution. Dissolution of drug from agglomerates is significantly more complex as compared to dissolution from primary particles, as it involves additional steps such as the wetting of agglomerates' surfaces, their sinking, dispersing in the liquid, and subsequent dissolution (Schubert 1993). Hence, the agglomerate dissolution is affected by several drug particle properties such as the agglomerate size, the primary particle size, hydrophobicity of the drug, the effective wettability, agglomerate dispersibility in a stirred dissolution medium, and so forth. Clearly, some of these properties are inter-related and their effects are confounding. For dry coated drug powders, the coating material properties greatly impact two critical underlying factors such as the particle cohesion, which governs their agglomerate size and dispersibility (Han et al. 2011; Ghoroi et al. 2013), and surface wettability of the coated particles. In terms of other key factors, primary drug particle size, its water solubility, and hydrophobicity are important.

Consequently, for this investigation, two poorly water soluble, model biopharmaceutical classification system (BCS) class II drugs that differ in their solubility and hydrophobicity are selected. The first choice is ibuprofen (Ibu), which has been the subject of previous reports. Two Ibu sizes are selected, Ibu20 ( $d_{50}$  20  $\mu m$ ) and Ibu10 ( $d_{50}$  10  $\mu m$ ). Selection of Ibu20 allows for comparing with previous results (Han et al. 2013a; Qu et al. 2015). The smaller sized Ibu10 allows assessing the size effect and the effect from the physicochemical properties by comparing to the second drug choice, griseofulvin (GF), comparable in size with Ibu10. GF is less hydrophobic as per its LogP value, but has higher melting point

and is less water-soluble hence slower dissolving. What makes GF even more interesting is its surface morphology, which as discussed in recent work, is macro-rough and does not exhibit as much cohesion reduction as other drug powders that are relatively smoother (Kunnath et al. 2021). This means that the effect of dry coating on GF in terms of agglomerate size reduction is expected to be lesser. Therefore, using GF in addition to Ibu20 or Ibu10 allows for testing our preliminary hypothesis that dissolution enhancement after silica coating, even hydrophobic silica, is possible largely due to significant reduction in active pharmaceutical ingredient (API) agglomeration after dry coating. As a corollary, when the API agglomeration cannot be reduced appreciably after dry coating, hydrophobic silica coating is unlikely to enhance dissolution performance. Consequently, these drug powders were dry coated with either hydrophobic or hydrophilic nano-silica at varying concentrations, normalized as theoretical surface area coverage (SAC) (Chen et al. 2008; Yang et al. 2005). Assessment of cohesion reduction was done through measuring powder flowability before and after dry coating. For measuring agglomerate sizes, two different dry dispersion methods, one with much gentler dispersion, were used. Wettability of the drug powders was evaluated using the modified Washburn method (Chander et al. 2007). The dissolution of the powders was determined as per USP (711) guideline, using USP IV method. To maximize discernment between dry coating formulations, de-ionized water was chosen as the dissolution medium owing to the model drugs' low solubility in water. The dissolution profiles were quantitatively analyzed by fitting the dissolution data via the Peppas model (Peppas 1985; Ritger and Peppas 1987). In addition, the area under the curve (AUC) for all dissolution profiles was evaluated to eliminate any issue with the applicability of the dissolution kinetics model. Finally, hydrophobicity and agglomerate sizes were assessed to better understand their potential dual impact on the dissolution of poorly soluble drugs after dry coating with hydrophobic or hydrophobic silica.

# 2. Materials and methods

#### 2.1. Materials

Griseofulvin (GF) was purchased from Hegno, China, and was use as received. It had a nominal mean particle size of  $10~\mu m$ . For obtaining Ibu20 and Ibu10, Ibuprofen 50 (Ibu50) (BASF, South Bishop, Texas 78343) as a starting material was milled down to suitable sizes. Physicochemical properties of these APIs are presented in Table 1. Typical SEM images of the uncoated drug particles, presented in Fig. 1(a), (f), and (k), demonstrate distinctly different surface morphology, with the GF exhibiting macro-scale roughness, where the surface asperities are about a micron or larger. In contrast, both Ibu10 and Ibu20 have relatively smoother surfaces. These observations are in line with the relative uniqueness of GF as reported in (Kunnath et al. 2021). Aerosil 200 (nano-sized hydrophilic fumed silica) and R972P (nano-sized hydrophobic fumed silica), donated by Evonik Corporation (Piscataway, NJ, USA), were selected as the dry coating agents due to their nano-sizes and relatively low surface energy values (Garg et al. 2015).

### 2.2. Methods

2.2.1. Surface energy analysis-Inverse Gas Chromatography
Surface energy assessment of the APIs and the silicas was done using

Table 1
Properties of APIs (Pubchem 2005).

API	Log P	Solubility in water at STP (mg/L)	Melting Point at 1 atm (°C)
Ibuprofen20	3.9	21	75–77
Ibuprofen10	3.9	21	75–77
Griseofulvin	2.18	8.64	220

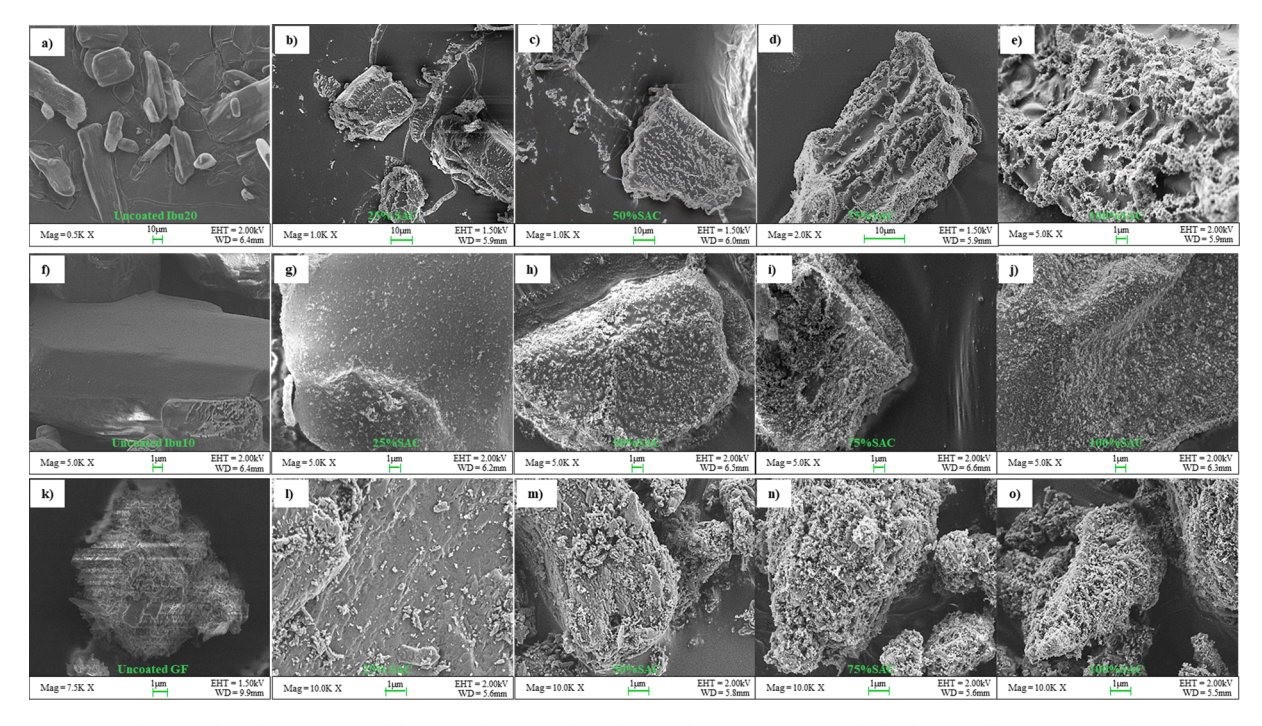


Fig. 1. SEM images of uncoated and R972P coated drug powders. For ibuprofen20 (Ibu20): (a) uncoated, (b) theoretical SAC25%, (c) theoretical SAC50%, (d) theoretical SAC75%, and (e) theoretical SAC100%. For ibuprofen10 (Ibu10): (f) uncoated, (g) theoretical SAC25%, (h) theoretical SAC50%, (i) theoretical SAC75%, and (j) theoretical SAC100%. For griseofulvin (GF): (k) uncoated, (l) theoretical SAC25%, (m) theoretical SAC50%, (n) theoretical SAC75%, and (o) theoretical SAC100%.

an automated Inverse Gas Chromatography (Surface Measurement System Ltd., Middlesex, UK) with a flame ionization detector (FID). The details of the sample preparation method as well as the conditioning were as previously employed (Han et al. 2013b; Chen et al. 2018a). Hexane, heptane, octane, nonane, and decane were selected as the nonpolar probes to measure dispersive surface energy. Dichloromethane and ethyl acetate were chosen as the polar probes for evaluating the polarity (Han et al. 2013b; Chen et al. 2018a). The infinite dilution method was employed with the fractional probe surface area coverage fixed at 0.03 (Han et al. 2013b; Chen et al., 2018a,b).

#### 2.2.2. Preparing milled Ibu via fluidized energy mill (FEM)

The mean particle size of as received Ibu50 was reduced by milling in a fluid energy mill (FEM) to 20  $\mu$ m in a manner similar to previous studies (Han et al. 2011). At a fixed feeding rate of 6 g/min, Ibu50 was fed by employing a volumetric feeder (Schenck Process GmbH, WI, USA) to the FEM. The feeding and grinding pressures were set to be 25 psi and 20 psi, respectively (Han et al. 2011). Likewise, Ibu10 was prepared by milling Ibu50 at a fixed feeding rate of 5 g/min while setting the feeding and grinding pressures at 30 and 25 psi, respectively (Han et al. 2011).

# 2.2.3. Dry coating: Ibu and as-received GF via LabRAM

Ibuprofen (Ibu) and griseofulvin (GF) are two model biopharmaceutical classification system (BCS) class II drugs. For coating materials, silica R972P and silica A200 are used as model hydrophobic and hydrophilic additives, respectively. They are used for consistency in terms of their main mechanism of reduced cohesion, which is attributed to the creation of nano-scale surface roughness after coating while having greatly differing hydrophobicity levels (Chen et al. 2018a; Chen et al. 2008; Huang et al. 2017; Kunnath et al. 2018; Yang et al. 2005).

Each API was dry coated into the eight different dry coating formulations using a high-energy vibratory mixer, LabRAM (Resodyn, USA) due to the ease of operation and short processing time. It is noted that LabRAM is a convenient material sparing device. Unfortunately, it may not be as industry relevant as the comil or fluid-energy mill, which have both been used to achieve similar performance as the Lab RAM

(Chen et al. 2020; Chen et al. 2018b). The vibrational intensity was set at 75-times gravitational force with 5 min mixing time to ensure uniform silica coating onto the surface of drug particles as per previous work (Huang et al., 2015a,b; Huang et al. 2017). The amounts of silica that correspond to theoretical surface area coverage (SAC) of the API particles are provided in Table 2. The weight percent of silica required to achieve 100% SAC was based on the Sauter mean particle size  $d_{3,2}$  of the API following the assumptions presented previously (Chen et al. 2008;

**Table 2**Formulation details for dry coated ibuprofen20 (Ibu20), ibuprofen10 (Ibu10), and griseofulvin (GF).

Sample ID	drug % (w/ w)	R972P % (w/ w)	Sample ID	drug % (w/ w)	A200 % (w/ w)
Ibu20-R972P-	99.46	0.54	Ibu20-A200-	99.72	0.28
25SAC			25SAC		
Ibu20-R972P-	99.01	0.99	Ibu20-A200-	99.45	0.55
50SAC			50SAC		
Ibu20-R972P-	98.47	1.53	Ibu20-A200-	99.17	0.83
75SAC			75SAC		
Ibu20-R972P-	97.70	2.30	Ibu20-A200-	98.90	1.10
100SAC			100SAC		
Ibu10-R972P-	99.08	0.92	Ibu10-A200-	99.48	0.52
25SAC			25SAC		
Ibu10-R972P-	98.16	1.84	Ibu10-A200-	98.97	1.03
50SAC			50SAC		
1Ibu10-R972P-	97.24	2.76	Ibu10-A200-	98.45	1.55
75SAC			75SAC		
Ibu10-R972P-	96.32	3.68	Ibu10-A200-	97.93	2.07
100SAC			100SAC		
GF-R972P-	99.43	0.57	GF-A200-	99.68	0.32
25SAC			25SAC		
GF-R972P-	98.86	1.14	GF-A200-	99.36	0.64
50SAC			50SAC		
GF-R972P-	98.28	1.72	GF-A200-	99.04	0.96
75SAC			75SAC		
GF-R972P-	97.71	2.29	GF-A200-	98.72	1.28
100SAC			100SAC		

Yang et al. 2005). For dry coating, pre-determined masses of API and silica were placed in a 300 mL plastic jar, and the LabRAM was operated as mentioned above to achieve dry coating.

#### 2.2.4. Field Emission Scanning electronic Microscope (FESEM)

Small quantities of powder samples, secured by a double-sided carbon type, were placed on an aluminum stub. The excess powder was removed by compressed air before carbon coating (Q150T 16017, Quorum Technologies Ltd, Laughton, East Sussex, England). All powder samples were carbon-coated to enhance electron conductivity for better imaging. A Field Emission Scanning Electron Microscope (FESEM) (EM JSM-7900F, JEOL Ltd., USA) was used to assess the quality of dry coating and dry coating efficiency by inspecting targeted particle surface morphology for each formulation.

# 2.2.5. Particle sizing via laser diffraction after dry dispersion in air

The volume-based particle size distribution statistics including  $d_{10}$ ,  $d_{50}$ ,  $d_{90}$ , and  $d_{3,2}$  of processed powders were measured by utilizing Sympatec Helos/Rodos laser diffraction particle size analyzer (Sympatec Inc., NJ). Before primary particle size evaluation, a dispersion pressure titration was conducted by varying the pressure from 0.1 to 2 bar with an increment of 0.5 bar. The lowest compression pressure was used possibly to capture the presence of agglomerates. However, as reported by the previous work (Huang et al. 2017), even at the gentlest dispersion pressure, 0.1 bar, the particles were deagglomerated. See Supplementary material, Table S1. Hence, Helos/Rodos laser diffraction particle size analyzer was employed to measure primary particle sizes only, at the dispersion pressure of 1.0 bar, the dispersion pressure which resulted in the most consistent particle size distribution measurements as other studies prove (Huang et al. 2017; Kunnath et al. 2018). For each sample, at least triplicates of measurements were taken.

2.2.6. Particle sizing via dynamic image analysis after dry dispersion in air The extent of agglomeration before and after dry coating was assessed by Sympatec QICPIC/GRADIS, a dynamic imaging particle sizer (Sympatec Inc., NJ) (Zakhvatayeva et al., 2018; Zuo et al., 2019). Unlike Sympatec RODOS/HELOS, QICPIC/GRADIS captures the particle images for both size and shapes analysis as the powders fall through a 50 cm long shaft via gravity (Zakhvatayeva et al., 2018; Zuo et al., 2019). While falling, the camera captures 2-D images of powder in real-time and converts the image data to measurement data. Since powder dispersion relies only on gravity, the employment of QICPIC/GRADIS is expected to impart a significantly lower level of deagglomeration force as compared to RODOS/HELOS, allowing more sensitive discernment of changes in agglomerate sizes after the dry coating. Therefore, the current study assessed the agglomerates of each API before and after dry coating by utilizing this instrument. To ensure repeatability, at least five repeated measurements were taken for each powder sample.

#### 2.2.7. Powder characterization using FT4 powder tester

The current study employed the Freeman FT4 powder tester (Freeman Technologies Ltd., Worcestershire, UK) to evaluate the bulk density and flow function coefficient (FFC). FFC is the ratio of major principal stress to the unconfined yield stress. The previous publications (Chen et al. 2018a; Chen et al. 2008; Freeman 2007; Jallo et al. 2012; Yang et al. 2005) explained detailed test procedures for bulk density and shear stress measurements. In the present study, 3 kPa was selected to be the pre-consolidation pressure for evaluating FFC. The flowability of the tested powders can be classified based on the calculated FFC values. This classification was defined by Schulze as the following: FFC < 1 - not flowing,  $1 < {\rm FFC} < 2$  - very cohesive,  $2 < {\rm FFC} < 4$  - cohesive,  $4 < {\rm FFC} < 10$  - easy flowing, and FFC > 10 - free-flowing (Schulze et al. 2008). In conjunction with FESEM image analysis, flowability measurement on the dry coated powder is another reliable method to evaluate the quality of the employed dry coating process on a quasi-quantitative scale.

#### 2.2.8. Liquid penetration in to agglomerates and the Washburn method

The physics of liquid infiltration into agglomerates has been studied for model agglomerates of uniform spheres with well-defined pore structures (see e.g. Bohin et al., 1994, 1995; Debacker et al., 2014). Liquid infiltrates into agglomerates due to capillary pressure,  $P_{\rm c}=2\gamma\cos\theta/r$ , generated by the small pores of the agglomerates. Here,  $\gamma$  is the liquid–air surface tension,  $\theta$  is the contact angle of the liquid on a solid surface, and r is the effective mean pore radius. Bohin et al. (1994, 1995) provides insights into the controlling parameters of liquid infiltration into "model spherical agglomerates". For the complete infiltration time  $t_{\rm max}$  of a spherical agglomerate of diameter  $D_{\rm a}$  and porosity  $\varepsilon$  that consists of primary particles with size  $D_{\rm p}$ , they proposed the following.

$$t_{max} = \frac{150D_a^2 \eta (1 - \varepsilon)}{36 \gamma \cos \theta D_p \varepsilon^2} \tag{1}$$

It was proposed that as the liquid infiltrates, the primary particles drag the infiltrating fluid with density  $\rho$  and dynamic viscosity  $\eta$ , causing a viscous resistance. Naturally, the model represented by Eq. (1) cannot fully account for all the complexities of this process such as agglomerate break-up that facilitates dispersion and dissolution (Alway et al. 1996; Galet et al. 2004; Yaremko et al. 2001), or dissolution of the primary particles, all of which alters the agglomerate structure. Nonetheless, Eq. (1) suggests that the agglomerate size, porosity and contact angle (hydrophobicity of the surfaces) are controlling parameters for wetting as well as drug dissolution—diffusion within the agglomerate pores, which are expected to modulate dissolution in agglomerated drug powders. The proposed study is intended to examine how dry coating materials affect the drug particle cohesion, hence the agglomerate size, and hydrophobicity of coated drug powders, all of which would impact their dissolution.

Towards that goal, the Washburn method allows for examining the hydrophobicity of powders by measuring liquid mass penetration of a wetting liquid through the voids of a packed powder bed via capillary action (Chander et al. 2007; Washburn 1921). Dictated by surface hydrophobicity of the packed powder bed and its geometric packing factor C, the squared mass m of liquid penetrating the bed as a function of time t is expressed as

$$m^2 = \left(\frac{C\rho^2\gamma\cos\theta}{\eta}\right)t\tag{2}$$

In Eq. (2),  $\eta$ ,  $\rho$ , and  $\gamma$  are the viscosity, the density, and the surface tension of the wetting liquid, respectively; C is a geometric packing factor;  $\theta$  is the surface contact angle; m is the total mass of the wetting liquid that penetrates through the packed bed. The data is recorded in m<sup>2</sup> vs. t, forming a straight line with a slope (( $C \rho^2 \gamma \cos \theta$ ) /  $\eta$ ) (Llusa et al. 2010). As the testing liquid penetrates a packed bed of testing drug, the wettability of the drug (Thakker et al. 2013; Washburn 1921) was assessed.

Attention Sigma 700 (Biolin Scientifin, Linthicum) was employed to measure the liquid penetration rate through the drug powder-packed bed. The testing powder holder consists of a perforated cylindrical metallic tube (Height: 10 cm and ID: 2 cm) and a hook at the top of the cover equipped with screw threads. After placing a paper filter (pore size 20 to 25  $\mu m$ ) at the perforated end of the metallic tube, packed 0.8 g of testing powder before each measurement by a spring to ensure uniform packing between the samples. A 30 mL beaker containing a presaturated liquid (either n-hexane as a reference liquid or deionized water) was placed below the perforated end of the tube. As the tip of the perforated end of the sample holder submerged (depth of submersion: 1.95 mm) in the liquid, Attention Sigma 700 recorded the mass of liquid penetrated the drug powder bed as a function of time. Geometric packing factor, C, was determined for each powder formulation by employing the reference liquid, the drug saturated n-hexane (Thakker et al. 2013; Li et al. 2017). The reference liquid completely wets the particle surface, setting the surface contact angle to  $0^\circ$  (cos  $\theta=1$ ). Since liquid properties and surface contact angles are known for the reference liquid penetration test (see Table 3), the slope of the liquid penetration curve was used to calculate C (Neirinck et al. 2010; Steele et al. 2008). The same experimental steps were repeated using the dissolution medium, de-ionized water, as the test liquid. As a standard approach, it was assumed that C for each powder sample remains the same when experiments with different liquids were performed. Hence, using the C value obtained from the test with the reference liquid and the slope of Eq. (2) from the test with the deionized water, the aqueous wettability,  $\cos\theta$ , was determined.

#### 2.2.9. Dissolution testing and dissolution kinetics

Adopting a flow-through cell dissolution apparatus (Sievens-Figueroa et al. 2012) (USP IV; Sotax, Switzerland) ensured simultaneous and efficient wetting of powder samples. 16 mL/min was the flow rate of the dissolution medium (deionized Milli-Q water) through the cells with an internal diameter of 22.6 mm. Following USP  $\langle 711 \rangle$  guideline, the temperature of the dissolution system was kept constant (37  $\pm$  0.5 °C). Two sets of glass filters (2.7  $\mu m$  pore size and 0.7  $\mu m$  pore size) were installed at the inlet and outlet of the cell to retain undissolved drug particles. Automated temporal sampling and analysis were performed using a Thermo Evolution UV spectrophotometer, which detects dissolved drug concentration in real-time. At the wavelength of 221 nm, dissolved Ibu was detected, and its absorbance was recorded per time. The recorded absorbance was converted to the concentration of dissolved Ibu using a pre-established calibration curve. The identical practice was taken for GF but the detection wavelength was 296 nm.

Measured and reported solubility of Ibu in de-ionized water was 21 mg/L at 25 °C (Yalkowsky 1992). Hence, to induce sink condition, 15 mg of Ibu was added to each cell, and each was connected to a 1 L of the de-ionized water reservoir (Liu 2008). During the experiment, the aqueous drug solution was agitated with a magnetic stirrer rotating at 500 rpm. Identical dissolution methodology and experimental setup were employed for GF as well. Since GF has a lower solubility in water than Ibu, 12.2 mg of GF was dissolved in 2 L of de-ionized water. The solubility of GF was reported as 8.64 mg/L at 25 °C and 14.5 mg/L at 37 °C (Yalkowsky 1992).

Dissolution data were fitted using the Korsmeyer–Peppas model (Peppas 1985; Ritger and Peppas 1987), which is expressed as

$$M_t/M_{\infty} = Kt^n \tag{3}$$

where  $M_{\infty}$  and  $M_t$  represent an initial mass of API powder added to a dissolution medium, and total mass of powder dissolved in the medium after time t, respectively; K denotes dissolution rate constant and n represents order of dissolution process.  $M_{\infty}$ ,  $M_t$ , and t are the experimentally measured values while K and n are the fitting parameters that account for various parameters of the system, including the pH, properties of the powders and dissolution media, surface area, and diffusional thickness. Eq. (3) describes both Fickian and non-Fickian diffusional release from either swellable or non-swellable polymeric delivery system.

As a simplified approach, n was assumed to be 0.43 for all formulations, the value which was assigned when spherical monodisperse particles dissolve in the Fickian system (Ritger and Peppas 1987). With n=0.43, K was fitted to the dissolution data. In all cases, the time series

**Table 3**Properties of testing liquids for the modified Washburn testing.

Liquid	Role	Density (kg•m <sup>-3</sup> )	Viscosity (mPa•s)	Surface tension (mN•m <sup>-1</sup> )
n-hexane	Reference liquid	661	0.32	18.0
De-ionized water	Test liquid	997	1.01	72.0

data till about 60% of the API was dissolved were studied to capture drug release kinetics (Peppas 1985; Ritger and Peppas 1987).

To minimize the impact of the discrepancy between the present system and the system considered in the original Peppas model, instead of just relying on the calculated dissolution rate constants, the area under the dissolution curve (*AUC*) values were also used as a complementary approach. As will be seen in Section 3, the trends in the dissolution rate constants were in line with the *AUC* trends for each formulation (Amidon et al.1995; Kortejärvi et al. 2007).

#### 3. Results and discussion

Each API was dry coated using LabRAM operated at fixed conditions. Various concentrations of hydrophobic or hydrophilic silica were used to investigate the impact of dry coating on agglomeration and surface hydrophobicity of the coated powders on the dissolution rate. Theoretical SAC % for each silica type on each API was varied in the increment of 25% from 25 to 100%. Considering the differing nature of each silica and the APIs, their compatibility was assessed using the total surface energy values based on the spreading coefficient of material B on material A (Wu 1973), see Eq. (4).

$$^{B/A}\lambda = 4\left[\frac{^{A}\gamma_{d} \quad ^{B}\gamma_{d}}{^{A}\gamma_{d} + \frac{^{B}\gamma_{d}}{^{A}\gamma_{p} + ^{B}\gamma_{p}} - \frac{^{B}\gamma_{p} + ^{B}\gamma_{d}}{2}\right] \tag{4}$$

In the above,  ${}^A\gamma_d$  and  ${}^B\gamma_d$  are the dispersive components, whereas  ${}^{A}\gamma_{p}$  and  ${}^{B}\gamma_{p}$  are the Lewis acid-base components of surface energy of two materials, respectively. Barra et al. (1998) considered both the influence of surface energy and particle size on the affinity of a binary mixture using the difference in the spreading coefficient  $A/B\lambda$ . In a later work, Jallo et al. (2011) proposed use of this difference to predict dry coating efficacy; when the difference is > 10, then the coating will be very good, when the difference is < 5, the dry coating will not be good, and when the difference is between 5 and 10, the coating will be achieved but will not be very good. Such difference for all pairs of host-guest combinations is calculated and shown in Table 4. Fortunately, the results indicate very good affinity for either of these silicas for all three APIs, hence dry coating efficacy is expected to be very good. SEM images of dry coated APIs also confirm that the silica particles are generally well-dispersed onto the surface of API particles, as shown in Fig. 1. For the sake of brevity, the images of the APIs coated with R972P are presented here although those for A200 coating were also comparable, see Fig. S1 in Supplementary Material.

In what follows, the impact of dry coating on the size of API agglomerates is assessed (Section 3.1), followed by an evaluation of the flowability of the powders (Section 3.2). The impact of dry coating on the wettability of API powders is discussed in Section 3.3, while dissolution profiles are presented in Section 3.4 to assess how API release was impacted by API agglomerate size and hydrophobicity of the API particles, noting both are expected to be affected by the type and theoretical SAC of the silica.

# 3.1. Size analysis of the coated and uncoated API powders

Laser diffraction size analysis using compressed dry air-based particle dispersion was employed for assessing primary particle size distributions (PSDs). In contrast, gentler gravity-based dispersion along with dynamic image analysis was used to evaluate agglomerate PSDs. Characteristic PSD values, i.e.,  $d_{10}$ ,  $d_{50}$ , and  $d_{90}$ , were measured and are presented in Table S1 in in *Supplementary Material* for dry coated Ibu20, Ibu10, and GF, whereas  $d_{90}$  values are provided in Table 5. Values measured with the compressed air dispersion showed no notable difference in size between uncoated and coated API samples, including those at varying silica concentration and type. In line with previous work (Huang et al. 2017), this dry dispersion method resulted in complete deagglomeration and allowed for the measurement of the primary

**Table 4**Affinity between APIs and the coating materials based on their total surface energy values.

	•	Dispersive energy (mJ/m <sup>2</sup> )	Polar energy (mJ/m²)	Total Surface energy (mJ/m²)	Affinity to R972P	Affinity to A200
	Ibu20	42.6	4.8	47.4	17.9	33.3
APIs	Ibu10	47.3	8.1	55.4	34.0	17.2
GF	GF	39.6	4.5	44.1	11.4	39.8
Castina mataniala	R972P	36.4	2.0	38.4		
Coating materials	A200	42.8	21.2	64.0		

particle sizes. Even for  $d_{90}$  measurements, no statistically significant differences are seen (Table 5). Thus, the state of agglomeration could not be assessed as was expected, likely because the API agglomerates are relatively soft and can easily be broken even at the lowest applied dispersion pressure. Fortunately, as seen in Table 5 and Supplementary Materials Table S2, the particle sizing with the gravity-dispersion in the air allowed better discernment of the differences in the API sizes before and after dry coating. Hence, those measurements were used to quantify the state of natural agglomeration.

# 3.2. Agglomerate size $(d_{90})$ and flowability as a function of silica SAC

The gravity-dispersion-based d<sub>90</sub> particle sizing as a measure of particle agglomeration (Table 5) demonstrated that agglomerates for dry coated APIs were much smaller than the agglomerates of uncoated APIs, which also had large standard deviations (SDs). Deagglomeration became more pronounced at higher silica loading, i.e., higher theoretical SAC. Further, lower SDs were observed than those of the uncoated powders. For better visualization of the relative agglomerate sizing for Ibu20, Ibu10, and GF, those values were normalized and presented in Fig. 2(a), (b), and (c), respectively. As shown, the agglomerate size reduction was  $\sim 15$  for dry coated Ibu20, and  $\sim 50$  for dry coated Ibu10, but was only ~ 4 for dry coated GF. For GF, that could be due to lesser cohesion reduction, which is in line with this tendency of GF as was recently observed (Kunnath et al. 2021). Agglomerate particle size ( $d_{90}$ ) and flowability (FFC) are related to the interparticle force (Capece et al. 2014; Han et al. 2013a; Jallo et al. 2012). Therefore, the flowability values were presented and normalized concerning their corresponding values for uncoated powders in Fig. 2. For the normalized agglomerate sizes, a smaller value indicates a greater extent of deagglomeration. Normalized flowability values are presented in terms of percentage increase in the FFC values. Numerical values of  $d_{90}$  and FFC before normalization, as well as powder cohesion, are listed in Table S4 of Supplementary Materials. For Ibu20 and Ibu10, the observed agglomerate reductions at various silica coatings were much higher than those for GF (also see Table 5). Likewise, the increased FFC values, also related to powder cohesion, were higher for Ibu20 and Ibu10, ranging from 0% to over 400% and 1000% for Ibu20 and Ibu10, respectively. A higher level of agglomerate size reduction for Ibu10 compared to Ibu20 at higher silica levels is in line with the dry coating impact. Whereas for GF, which is also fine sized, the increases in FFC were lower yet significant, but reaching only up to 40% because of its peculiar surface morphology (Kunnath et al. 2021). For dry coated Ibu20 powders, cohesion (see Supplementary Materials, Table S4) was reduced by up to 84%, improving the powder flowability from cohesive to well-flowing or even freeflowing. For Ibu10 powders, the cohesion was reduced by up to 93%, improving the flowability from the non-flowing to the free-flowing. Dry coated GF powders exhibited a maximum of 39% cohesion reduction, barely reaching the easy-flowing regime (FFC of 4 and higher) at 100% SAC. In summary, both the rheological powder testing and gravitydispersion-based size analyses confirm that for GF, the dry coating does not yield as drastic improvement as for Ibu20 or Ibu10, attributed to the intrinsic surface morphology of GF (Kunnath et al. 2021). Such dramatically different responses to dry coating for Ibu20 and Ibu10 versus GF may likely help confirm the hypothesis that dissolution enhancement after the hydrophobic coating is possible due to a

significant reduction in API agglomeration after the dry coating.

Regarding the effect of the types of silica, for Ibu20 and Ibu10, an increase in FFC for coating with hydrophobic silica (R972P) was greater than that for hydrophilic silica (A200); even 50% SAC R972P coating led to significant enhancement in FFC as well as agglomerate size reduction. Enhanced performance of R972P may be attributed to its lower dispersive surface energy, see Table 4 (Chen et al. 2018a). In summary, the agglomerate size reduction after dry coating with either silica type was more pronounced for both ibuprofen cases but not as pronounced for GF. Next, the effect of coating on the wettability of these powders was examined.

#### 3.3. Impact of coating on the wettability of coated API powders

The wettability of the dry coated samples was quantified by evaluating the contact angle of the powders by employing the modified Washburn method. The geometric packing factor C calculated from the hexane penetration data as well as the slope for the deionized water penetration and associated contact angle  $\theta$  are reported in Table 5. The further details of the liquid penetration experimental results including slope,  $R^2$ , and surface wettability are listed in Supplementary Materials Table S5. The modified Washburn equation fitted the  $m^2$ -t data for all powders well with  $R^2 \ge 0.94$ . As the concentration of R972P increased, all three cases of API powders exhibited lower surface wettability, as signified by a lower  $\cos\theta$  approaching 0 or  $\theta$  approaching 90°. Higher cosθ was calculated for the A200 dry coated API powder, indicating higher surface wettability. The results for wettability measurements, cosθ, are graphically presented in Fig. 3 as a function of theoretical SAC for coated Ibu20, Ibu10, and GF powders with R972P (hydrophobic silica) and A200 (hydrophilic silica). Interestingly, the uncoated Ibu10 and Ibu20 have dissimilar surface wettability, which could be due to a combined effect of their sizes and differences in their dispersive and polar surface energy values (Table 4) after dry milling. That might also be likely due to induced surface defects or increased higher surface energy surfaces, as observed previously, although such effects can be partially mitigated after dry (Han et al. 2013b). Uncoated Ibu10 wettability is very similar to GF, probably due to their size similarities. Overall, these results in Table 5 and Fig. 3 exhibit mostly expected trends except for Ibu10 at 25% SAC of A200 coating, which is most likely because even after the dry coating, there was no reduction in agglomerate size. In addition, the wettability after the dry coating appears to be independent of physicochemical differences in the APIs. Thus, the dry coating seemed to have the remarkable capability of modifying the target API's surface hydrophobicity based on the coating material's hydrophobicity and its concentration.

#### 3.4. Drug release from the uncoated and coated API powders

The dissolution profiles for the dry coated Ibu20, Ibu10, and GF, respectively, either with R972P or A200 coating, are presented along with a quantitative analysis of the results. Readers are reminded that deionized water was used as the dissolution medium for better discernment of the impact of dry coating, whereas previous studies involving the dry coating of Ibu used aqueous surfactant solutions; hence, the dissolution time scale was shorter for those studies (Han et al. 2011; Qu et al. 2015).

**Table 5**Agglomerate size evaluation and Modified Washburn based surface wettability evalution of the API powders.

Sample ID	Compressed Air	Gravity driven	Modified Washburn based evaluation			
	$d_{90}~(\mu\mathrm{m})$	$d_{90}~(\mu\mathrm{m})$	Coating material (w/w, %)	Packing factor C (m <sup>5</sup> )	Surface contact angle (°)	
Uncoated Ibu20	52.3±0.47	1050.6±553.75	_	$8.54 \times 10^{-14}$	70	
Ibu20-R972P-25SAC	$49.0 \pm 0.33$	$467.2 \pm 556.24$	0.54	$4.07 \times 10^{-16}$	80	
Ibu20-R972P-50SAC	49.4±0.29	$66.8 \pm 6.34$	0.99	$8.14 \times 10^{-16}$	84	
Ibu20-R972P-75SAC	$48.2 {\pm} 0.18$	59.7±3.35	1.53	$1.22\times10^{-15}$	88	
Ibu20-R972P-100SAC	46.6±0.16	$56.1 \pm 2.42$	2.3	$1.63\times10^{-15}$	89	
Ibu20-A200-25SAC	$46.0 \pm 0.50$	$263.0{\pm}154.23$	0.28	$2.20\times10^{-16}$	69	
Ibu20-A200-50SAC	46.5±0.47	74.6±5.85	0.55	$4.07 \times 10^{-16}$	66	
Ibu20-A200-75SAC	$45.1 {\pm} 0.54$	$73.7 \pm 6.77$	0.83	$4.27 \times 10^{-16}$	66	
Ibu20-A200-100SAC	$46.2 \pm 0.32$	70.5±4.85	1.1	$4.19\times10^{-16}$	63	
Uncoated Ibu10	$31.3 {\pm} 0.20$	$1368.5 \pm 818.31$	_	$2.93\times10^{-16}$	82	
Ibu10-R972P-25SAC	$32.8 {\pm} 0.10$	$460.4 \pm 295.38$	0.92	$2.01 \times 10^{-15}$	86	
Ibu10-R972P-50SAC	$31.7 {\pm} 0.21$	$43.8{\pm}1.95$	1.84	$3.26\times10^{-15}$	87	
Ibu10-R972P-75SAC	$31.2 {\pm} 0.24$	$42.0 \pm 0.73$	2.76	$4.33\times10^{-15}$	88	
Ibu10-R972P-100SAC	$31.7 {\pm} 0.05$	42.0±1.70	3.68	$1.14\times10^{-14}$	89	
Ibu10-A200-25SAC	$30.8 {\pm} 0.18$	$1427.5 \pm 625.57$	0.52	$1.73 \times 10^{-15}$	82	
Ibu10-A200-50SAC	$30.6 {\pm} 0.35$	$1100.6 \pm 323.33$	1.03	$2.79\times10^{-15}$	65	
Ibu10-A200-75SAC	$29.6 {\pm} 0.12$	$983.9 \pm 301.34$	1.55	$4.18\times10^{-15}$	59	
Ibu10-A200-100SAC	$29.4{\pm}0.24$	49.2±3.96	2.07	$5.42\times10^{-15}$	55	
Uncoated GF	$21.5 {\pm} 0.69$	$968.2 \pm 446.16$	_	$8.14 \times 10^{-17}$	81	
GF-R972P-25SAC	$21.3 {\pm} 0.95$	$623.3 \pm 360.01$	0.57	$1.22\times10^{-16}$	88	
GF-R972P-50SAC	$20.9 {\pm} 0.38$	$579.8 \pm 437.65$	1.14	$2.03\times10^{-16}$	90	
GF-R972P-75SAC	$20.7 {\pm} 0.13$	$309.8 \pm 215.91$	1.72	$8.14\times10^{-16}$	90	
GF-R972P-100SAC	$20.1 {\pm} 0.07$	$267.3 \pm 196.75$	2.26	$1.22\times10^{-15}$	90	
GF-A200-25SAC	$21.4 {\pm} 0.85$	$765.1 \pm 415.14$	0.32	$1.63\times10^{-16}$	79	
GF-A200-50SAC	$21.4 {\pm} 0.23$	604.3±378.04	0.64	$2.03 \times 10^{-16}$	78	
GF-A200-75SAC	$21.4 {\pm} 0.05$	$293.5 \pm 249.20$	0.96	$8.14 \times 10^{-16}$	77	
GF-A200-100SAC	$21.2 {\pm} 0.20$	172.8±64.44	1.28	$4.07 \times 10^{-16}$	77	

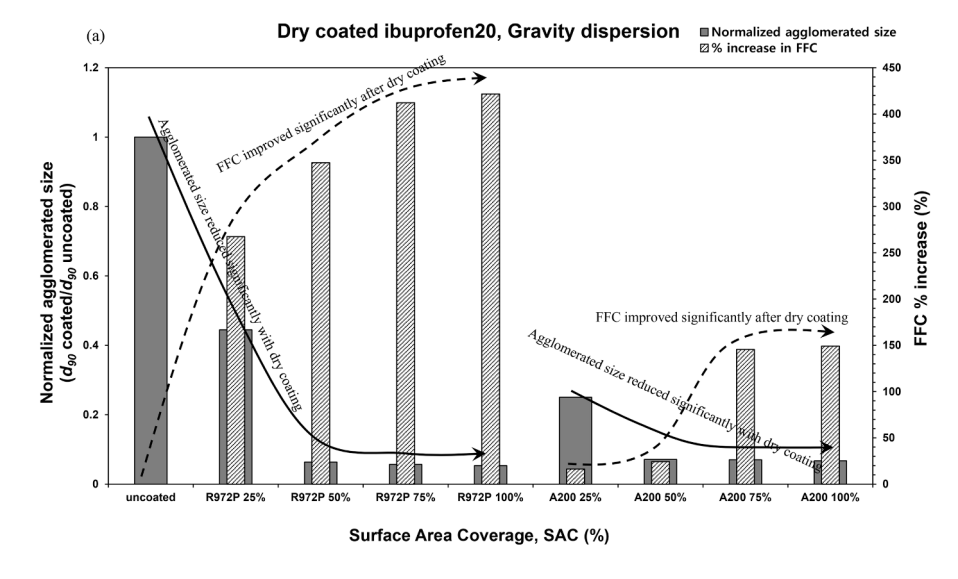
# 3.4.1. API release from the uncoated and coated Ibu20 and Ibu10

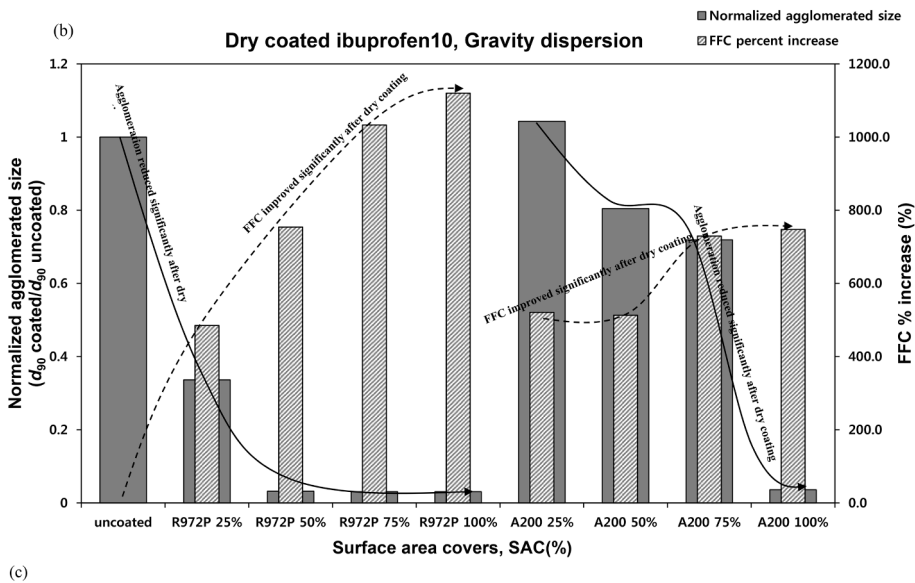
The dissolution profiles in Fig. 4 illustrate that Ibu20 dry-coated with various SAC of R972P (hydrophobic silica) exhibited faster API release for the first  $\sim 300$  min than uncoated Ibu20. From the highest to the lowest, the order of dissolution enhancement was ranked in terms of SAC: 50% > 75% > 100% > 25%. For all coated Ibu20 powders, the dissolution profiles exhibited a significant slow-down (shallower slope) after 300 min, which became very apparent at 75% and 100% SAC. This pattern can also be seen in the API release % values after 900 min shown in Table 6 (also see *Supplementary Materials* Fig. S3 (a)).

The observed counterintuitive API dissolution rate improvement after dry coating Ibu20 with hydrophobic R972P may be better understood by considering two opposing effects: agglomerate size reduction and enhanced hydrophobicity (reduced wettability). As discussed in Section 3.2 (refer to Table 5 and Fig. 2(a)), as R972P loading (SAC) increased, the agglomerate sizes for the coated Ibu20 powders decreased significantly. However, such an increase in SAC of R972P led to lower  $\cos\theta$ , i.e., the decreased surface wettability of Ibu20 particles (refer to Fig. 3). These two counteracting effects could explain significantly improved dissolution rate at an intermediate level of R972P coating, which appears to be 50% SAC for which the reduced agglomeration effect seems to outweigh increased hydrophobicity (see Fig. 2(a)). Reduced agglomeration itself reduces the apparent particle size, which would generally lead to faster dissolution. In addition, Eq. (1) helps understand another important effect due to reduced agglomerate sizes, since it implies faster penetration and faster complete immersion (lower  $t_{\rm max}$ ) of API agglomerates by the dissolution medium (Shubert 1993). At the same time, it also predicts that immersion takes longer for more hydrophobic agglomerates. Hence, even though Eq. (1) represents a highly simplified model, it outlines the underlying physics behind these two opposing effects of R972P coating. It is expected that faster immersion affects the dispersion of the agglomerates in the dissolution medium and thus the dissolution rate. In summary, these competing effects explain the enhanced dissolution of Ibu20 at an intermediate coating level, i.e., 50% SAC, of R972P. It is useful to note that this level of coating is equivalent to the amount of hydrophobic silica used in previous work, i.e., 1 w/w % R972P, which also reported significant dissolution improvement of Ibu20 even with hydrophobic silica coating (Ou et al. 2015).

Hydrophobic silica R972P dry coated Ibu10 exhibited similar trends as those observed with R972P dry coated Ibu20 (See Fig. 5 and Table 6). However, only within the initial 100 min of the dissolution process, all the dry coated Ibu10 powders showed faster release than the uncoated Ibu10 powder. As the dissolution process progressed beyond 100 min, the release rates decreased, showing slower Ibu release rates than that of uncoated Ibu10, except for R972P of 25% SAC. The dissolution rate was slowest for R972P of 100% SAC, followed by 50% SAC and 75% SAC. R972P of 50% and 75% SAC showed no noticeable differences in their release rates throughout the dissolution process. As was the case with Ibu20, when 1 w/w% of R972P was used for dry coating Ibu10, which is equivalent to 25% SAC, the dissolution rate was significantly improved (Fig. 5 and Table 6). Both Ibu20 R972P 50% SAC and Ibu10 R972 25% SAC samples show such intriguing results (refer Supplementary materials, Fig. S3(a) and (b)), in line with (Qu et al. 2015). Thus, for R972P dry coated Ibu20 and Ibu10, 1 w/w% of R972P (50% SAC and 25% SAC for Ibu20 and Ibu10, respectively) appeared to be the right concentration of hydrophobic silica. That was when the agglomerate size reduction effect outweighed the impact from the reduction in surface wettability, hence enhancing the dissolution rate of Ibu.

In contrast to the R972P coating, the hydrophilic silica A200 coated





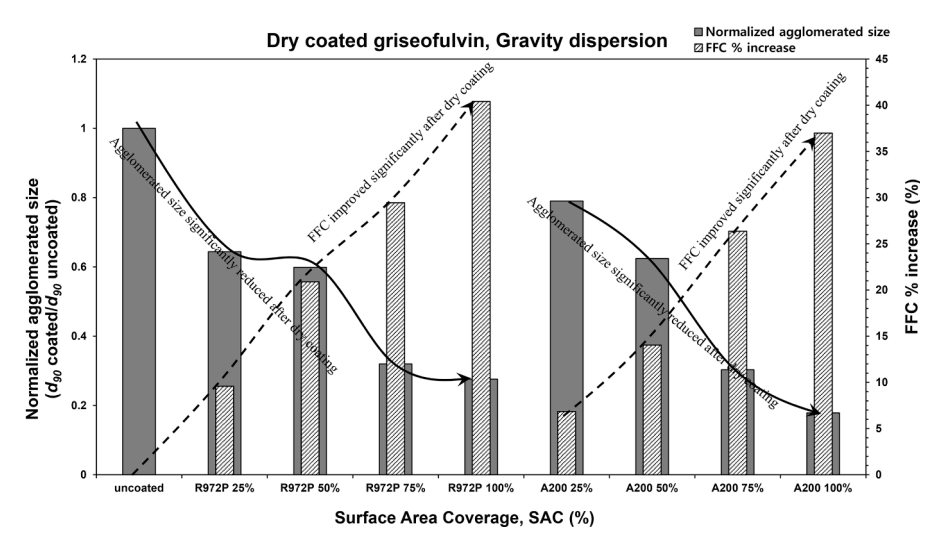


**Fig. 2.** Normalized agglomerated particle size ( $d_{90}$  coated /  $d_{90}$  uncoated), in relation to percent FFC increase after dry coating, measured using gravity driven dispersion method for (a) dry coated ibuprofen20 (Ibu20), (b) dry coated ibuprofen10 (Ibu10), and (c) dry coated griseofulvin (GF).

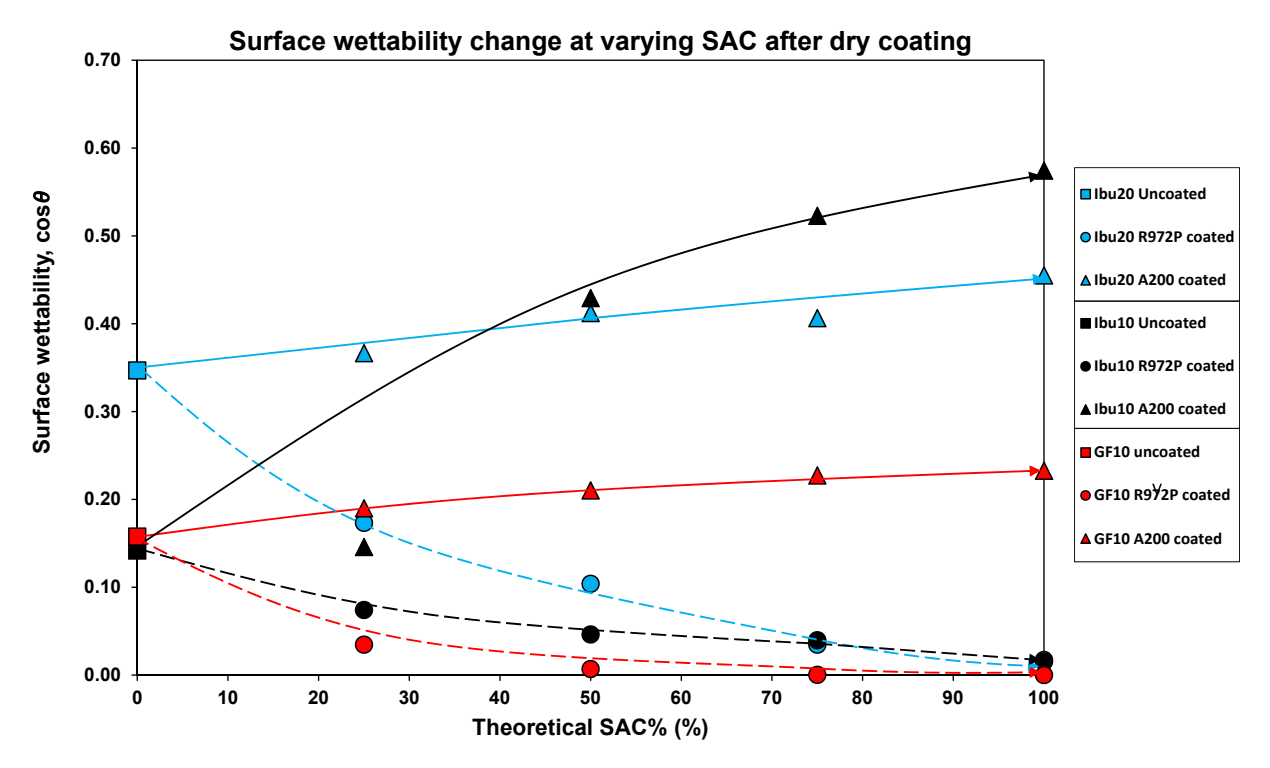


Fig. 3. Surface wettability (cosθ) at varying silica coating surface area coverage, SAC %, for dry coated Ibu20, dry coated Ibu10, and dry coated GF. Trend lines are only illustrative and do not represent a fitted model.

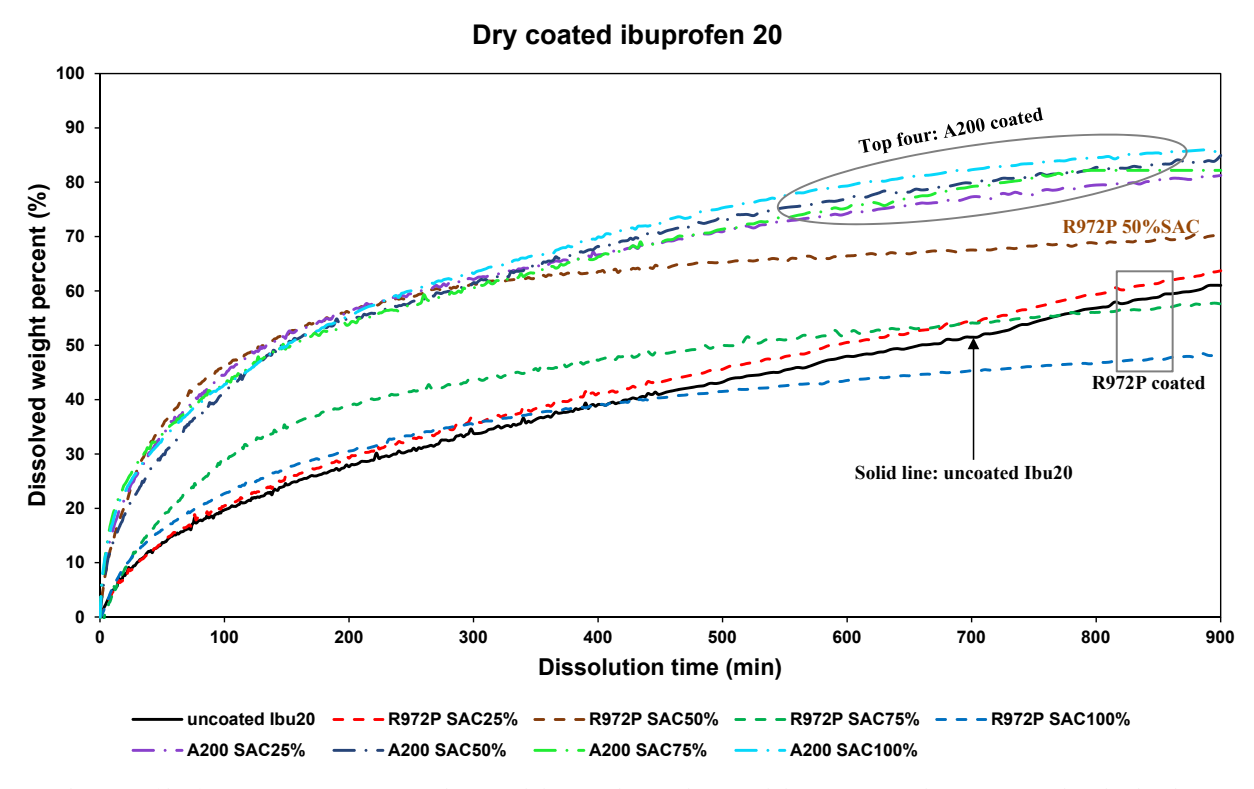


Fig. 4. Dissolution profiles from UPS IV testing; R972P dry coated Ibu20 and A200 dry coated Ibu20. De-ionized water was used as the dissolution medium.

Ibu20 did not exhibit such opposing effects since being hydrophilic, both the effects, agglomerate size reduction, and surface wettability was additive. Accordingly, as the SAC of A200 increased, it led to a monotonic reduction of agglomerate size (see Table 5) as well as a monotonic increase in wettability (higher cosθ, see Fig. 3). Hence, for all A200 dry coated cases, the rates of Ibu20 release were significantly higher than

that of the uncoated Ibu (Fig. 4), although beyond 25% coating SAC, its effect became marginal. These results agree with those in (Han et a. 2011), where although the effect of different silica amounts was not explored, significant dissolution rate improvement after dry coating with hydrophilic silica was noted. A quick examination of Fig. 3 and Table 5 revealed a dramatic decrease of the surface wettability  $(\cos\theta)$ , up

Table 6 Total percentage drug dissolved and the dissolution rate constant at the fixed edissolution rate equation exponent (n = 0.43) for the uncoated and coated API powders.

Sample ID	Total drug di	ssolved after 900 min	Dissolution rate constant at fixed rate exponent, $n$		
	Dissolved percent (%)	Dissolved percent change (%)	Time range	Dissolution rate constant $K \text{ (min}^{-0.43}\text{)}$	$R^2$
Uncoated Ibu20	61.0 ±3.7	-	0 to 900 min	0.030	0.996
Ibu20-R972P-25SAC	$63.7 \pm 7.7$	+ 4.4	0 to 900 min	0.031	0.996
Ibu20-R972P-50SAC	$70.3 \pm 8.2$	$+\ 15.2$	0 to 900 min	0.048	0.971
Ibu20-R972P-75SAC	$57.6 \pm 5.4$	- 5.6	0 to 900 min	0.035	0.992
Ibu20-R972P-100SAC	$48.4\pm2.2$	- 20.7	0 to 900 min	0.029	0.995
Ibu20-A200-25SAC	$81.3 \pm 4.9$	+ 33.3	0 to 300 min	0.058	0.997
Ibu20-A200-50SAC	84.9 $\pm 6.6$	+ 39.2	0 to 300 min	0.056	0.999
Ibu20-A200-75SAC	$\textbf{82.2} \pm \textbf{7.9}$	+ 34.8	0 to 300 min	0.057	0.996
Ibu20-A200-100SAC	$86.2 \pm 4.1$	+ 41.3	0 to 300 min	0.058	0.999
Uncoated Ibu10	$70.2{\pm}5.1$	-	0 to 900 min	0.035	0.984
Ibu10-R972P-25SAC	75.1±7.7	+ 6.9	0 to 900 min	0.044	0.997
Ibu10-R972P-50SAC	49.4±5.9	- 29.7	0 to 900 min	0.030	0.992
Ibu10-R972P-75SAC	51.8±5.4	- 26.2	0 to 900 min	0.032	0.993
Ibu10-R972P-100SAC	$38.6 {\pm} 7.2$	<b>- 45.0</b>	0 to 900 min	0.022	0.993
Ibu10-A200-25SAC	81.0±7.7	+ 15.4	0 to 300 min	0.049	0.994
Ibu10-A200-50SAC	89.4±4.0	+ 27.3	0 to 300 min	0.048	0.995
Ibu10-A200-75SAC	$86.5{\pm}6.1$	+ 23.2	0 to 300 min	0.058	0.999
Ibu10-A200-100SAC	85.7±5.9	+ 22.1	0 to 300 min	0.077	0.991
Uncoated GF	$\textbf{72.6} \pm \textbf{0.03}$	-	0 to 300 min	0.054	0.994
GF-R972P-25SAC	$42.7\pm6.7$	- 41.2	0 to 900 min	0.025	0.983
GF-R972P-50SAC	$22.1\ \pm10.3$	- <b>69.6</b>	0 to 900 min	0.012	0.996
GF-R972P-75SAC	$20.6 \pm \! 6.1$	<b>- 71.6</b>	0 to 900 min	0.011	0.998
GF-R972P-100SAC	$17.5 \pm 4.8$	<b>- 75.9</b>	0 to 900 min	0.009	0.979
GF-A200-25SAC	$76.4 \pm 6.6$	+ 5.2	0 to 160 min	0.068	0.990
GF-A200-50SAC	$74.8 \pm 14.0$	+ 3.0	0 to 265 min	0.056	0.990
GF-A200-75SAC	$81.2 \pm 3.6$	+ 11.8	0 to 155 min	0.065	0.993
GF-A200-100SAC	$82.2 \pm \hspace*{-0.05cm} \pm \hspace*{-0.05cm} 13.0$	+ 13.2	0 to 125 min	0.070	0.987

to 95% (refer to Table 5) of Ibu20 after coating with the hydrophobic silica (R972P), whereas showing a maximum of 31% increase after coating with the hydrophilic silica (A200). That implies that the surface wettability impact of the A200 coating was relatively insensitive to the SAC level compared to the R972P coating. Similarly, the dependence of the reduction of the normalized  $d_{90}$  on A200 SAC was also weak (see Table 5).

The dissolution profiles of hydrophilic A200 dry coated Ibu10, Fig. 5, indicate that the dissolution rates increased in the order of increasing % SAC, with noticeable improvement for all cases. The most visible difference between A200 dry coated Ibu10 and Ibu20 from both Fig. 4 and Fig. 5 is that for Ibu10, % SAC seemed to have a noticeable influence on the dissolution rate, especially at the early stage of the dissolution process. Referring to the particle size measurement results (Table 5) and the surface wettability evaluation results (Table 5 and Fig. 3, Supplementary Materials Table S5), the enhanced dissolution upon A200 dry coated Ibu10 could have resulted from both the effective reduction in the agglomerated particle size and improved surface wettability, hence the faster wetting and dissolution medium penetration into the agglomerates. Further, faster penetration into smaller agglomerates could weaken the agglomerate structure, which could facilitate breakage of the agglomerates during the dissolution and thus faster drug release, all of which could be additive (Forny et al. 2011; Ji et al. 2016). As A200 coating increased, the gradual reduction in the gravity-dispersion-based agglomerated size (Table 5 and Supplementary Materials Table S2) for Ibu10 was observed. In contrast, for Ibu20, the agglomerated size ( $d_{90}$ ) did not change with SAC above 50% SAC. These observations are in line with the dissolution profiles for both Ibu10 and Ibu20, indicating that the agglomerate size is driving the dissolution rate after dry coating with

a hydrophilic coating material. Overall, both the agglomerate size and surface hydrophobicity of the coating material have a significant impact on the dissolution rate.

#### 3.4.2. API release from the uncoated and coated GF

The dissolution profiles of GF dry coated with R972P and A200 are presented in Fig. 6. In contrast to Ibu, a higher % SAC of hydrophobic silica R972P monotonically led to the slower dissolution of GF. Although there could be some positive effects of the reduced agglomeration after dry coating, the impact from increased surface hydrophobicity may have been dominating (refer to Fig. 3). In summary, when the impact of agglomerate size reduction due to the reduced cohesion is low, the dissolution is mainly driven by the surface hydrophobicity or wettability, which is the case for GF. Whereas for Ibu10 and Ibu20, the dry coating is very effective in both the cohesion reduction and agglomerate size reduction for either silica (refer to Table 5 and Supplementary Materials, Table S4), hence they demonstrate this unique behavior. While outside the scope of the current manuscript, a mechanistic understanding of when dry coating works better is an area worthy of future investigations.

# 3.4.3. Quantification of dissolution profiles at varying SAC%

As discussed before, considered two approaches to quantify the dissolution behavior. In the first approach, the Korsmeyer–Peppas model (Peppas 1985; Ritger and Peppas 1987) was used as an empirical fitting model with a fixed exponent in Eq. (3), n=0.43, to obtain an estimate of the drug dissolution rate. The second approach is to utilize the area under the curve (AUC), to avoid uncertainties in applying any rate equation including the one used here.

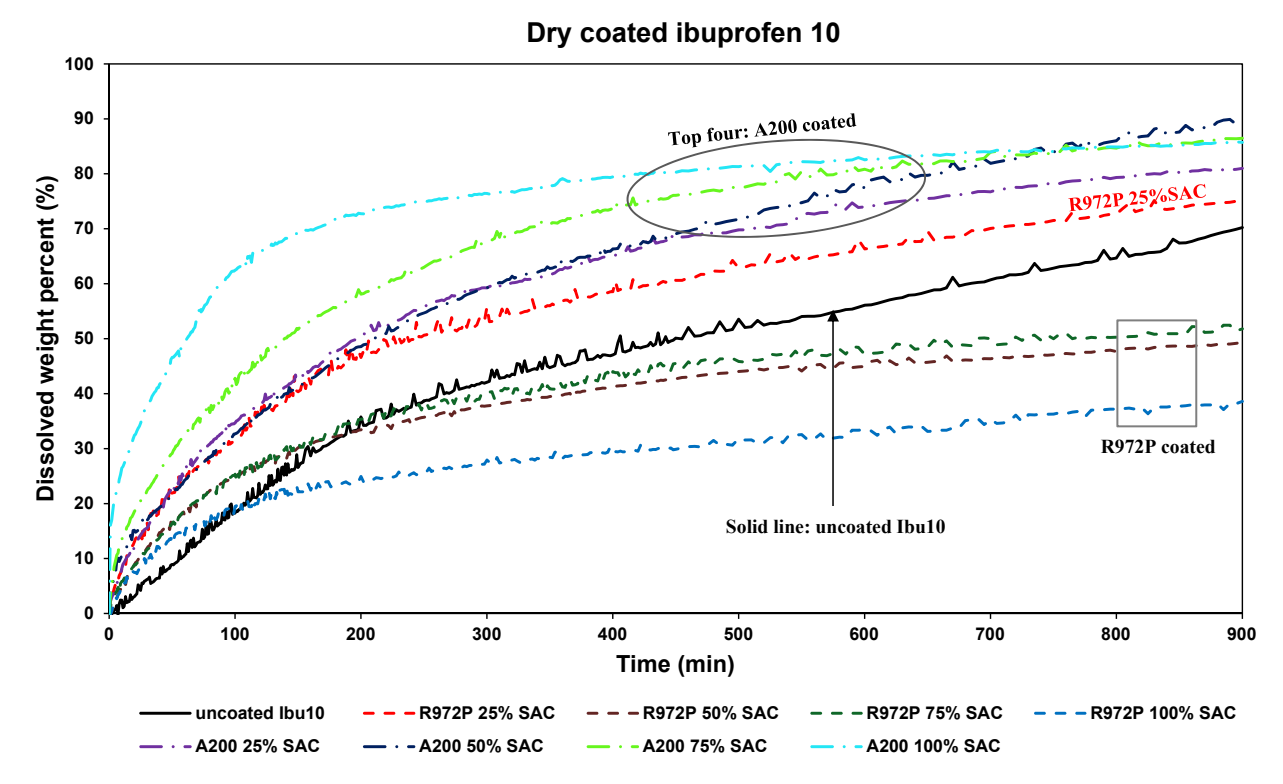


Fig. 5. Dissolution profiles from UPS IV testing; R972P dry coated Ibu10, and A200 dry coated Ibu10. De-ionized water was used as the dissolution medium.

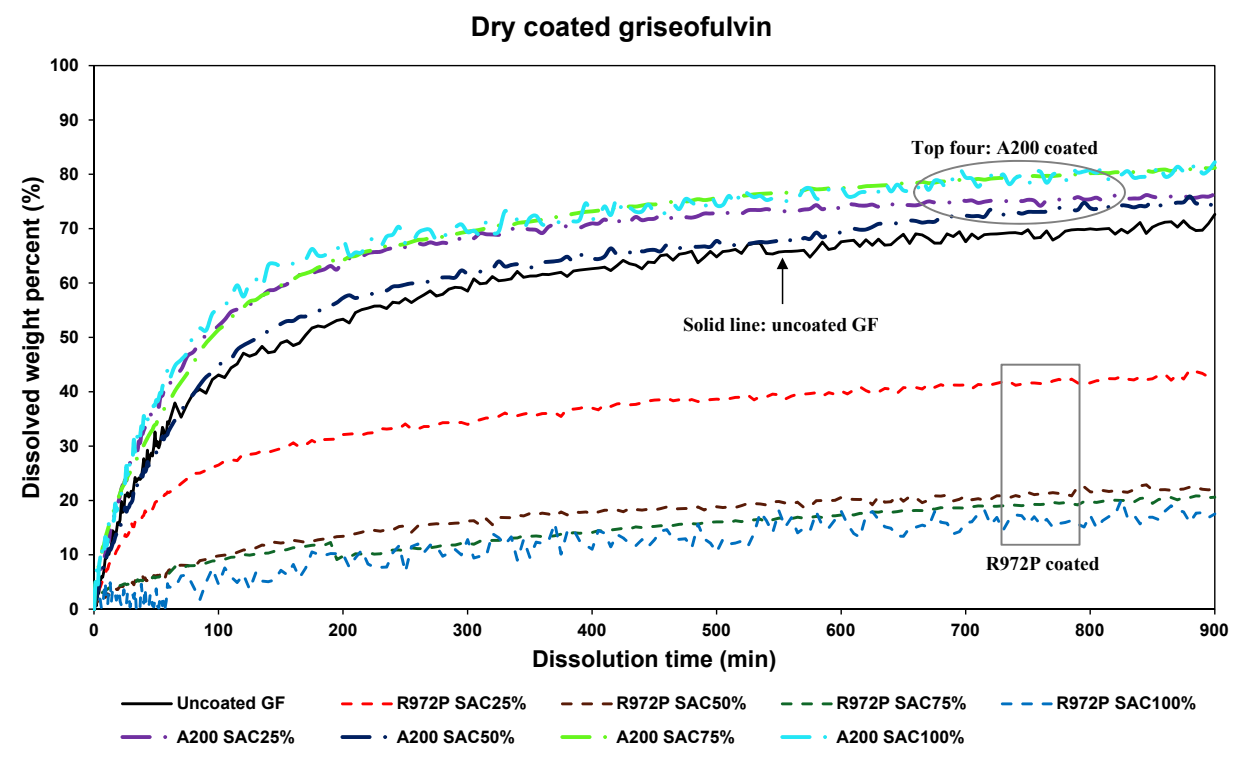


Fig. 6. Dissolution profiles from UPS IV testing; R972P dry coated GF, and A200 dry coated GF. De-ionized water was used as the dissolution medium.

Using the first approach, the estimated dissolution rate constant K and  $R^2$  for all cases are presented in Table 6. The time-series data, shown in the second column, for each case was selected such that about 60% of the drug was dissolved. Based on the  $R^2$  values, the fits are excellent for all cases indicating that the model is very reasonable. Estimated values

for K as a function of silica SAC for Ibu20, Ibu10, and GF, are plotted in Fig. 7. For Ibu20, K increased with the hydrophilic silica (A200) coating at as little as 25%, which leveled off as the SAC was increased further (Fig. 7). Thus, 25% SAC appeared to be sufficient for enhancing the surface wetting of dry coated Ibu20 particles. In contrast, for Ibu10,

although 25% SAC with A200 improved K, it kept increasing beyond 25% SAC, most likely because the agglomerate size of Ibu10 continued to decrease with higher % SAC (Table 5). Whereas for Ibu20, agglomerate sizes significantly reduced at 50% SAC beyond which the impact was minimal. Thus, the quantitative evaluations based on K agree with the qualitative findings discussed in section 3.4.1.

For the hydrophobic silica (R972P) coating of Ibu20 and Ibu10, the outcomes are more intriguing, although in line with the qualitative findings where the highest K values occurred at the SAC of 50% and SAC of 25%, respectively. The highest K value is well in line with the dissolution profiles in Fig. 4.

For the second approach, the values for the area under the dissolution curve (dissolution AUC) from 0 to 900 min are plotted in Fig. 8 and follow the trends observed using the first approach where the dissolution rate constants for Ibu20 and Ibu10 with fixed n were considered. Hence, along with the qualitative trends, the dissolution kinetics represented by K values, the AUC results confirm the counterintuitive dissolution enhancements observed for Ibu10 and Ibu20 for hydrophobic silica coating.

The dissolution rate constants *K* for dry-coated GF present more intuitive trends (Fig. 7). For A200 coating, *K* increased monotonically with higher SAC, whereas for R972P coating, it decreased monotonically with higher SAC. The level of decrease in *K* due to R972P coating was higher than the level of increase in *K* due to A200 coating. This quantitative finding is in line with the qualitative observations in Section 4.3.2 and confirms that the overall dissolution driver for GF was surface wettability, which was dictated by the applied coating material. Combined with the wetting results (refer to Table 5 and Fig. 3), such behavior could have been anticipated from the agglomeration results in Table 5 and FFC results in Fig. 2 (also see *Supplementary Materials*, Table S4), demonstrating that the dry coating of GF was not as effective as those for Ibu20 and Ibu10.

The results shown in Fig. 7 were further substantiated by the *AUC* analysis presented in Fig. 8. As was the case for Ibu20 and Ibu10, the GF dissolution rate constants followed the same trends as the *AUC*.

3.4.4. Combined effect of the surface hydrophobicity and agglomerate size on the dissolution rate

The results so far indicate that the dissolution of dry coated API powders was affected by both the surface hydrophobicity and the reduction in agglomerate size. As mentioned before, the dissolution from an agglomerate is a multi-step process that includes wetting, sinking, penetration, dissolution, etc. (Schubert 1993). Therefore, it is a complex process that cannot be easily described by a simple model. Nonetheless, these two factors may be combined as the product of the wettability and available external specific surface area (SSA) of an agglomerate. Since the SSA is inversely proportional to the Sauter mean diameter  $d_{32}$  of the agglomerate measured by GRADIS, the combined effect could be captured by  $\cos\theta/d_{3,2}$ . Consequently, the dissolution for Ibu20, Ibu10, and GF are presented as a function of this product in Fig. 9 (a), 9(b), and 9(c), respectively.

For Ibu20, the combined effect is shown in Fig. 9(a) indicates that the product of the wettability and the extra-granular SSA of the agglomerate could capture the trends well. As could be expected, hydrophobic and hydrophilic silica behave differently, and that could be attributed to various complex phenomena (Schubert 1993), including the penetration of the dissolution media within the agglomerate, which could not be captured by  $\cos\theta/d_{3,2}$ . The most striking outcome is that the increased SSA effect well-compensates hydrophobicity effect for three different levels, 50%, 75%, and 25% SAC R972P silica coating, as the AUC for those cases is higher than for the uncoated Ibu20 shown as a filled square marker. While the 50% SAC R972P case, which is equivalent to 1 wt% silica, has the highest AUC, 25% SAC R972P silica coating appears to be an outlier, likely because its agglomerate size reduction was significantly lower than the other two SACs, see Fig. 2(a). The figure also shows that although the AUC for 50% SAC R972P coating is remarkably high, it barely reaches the level achieved after the lowest level of A200 coating. Further, the slopes of the trendlines for A200 and R972P are significantly different and may be driven by their wetting angles, the API sizes, and the API's solubility in the medium when Ibu20 is dry coated with hydrophilic silica.

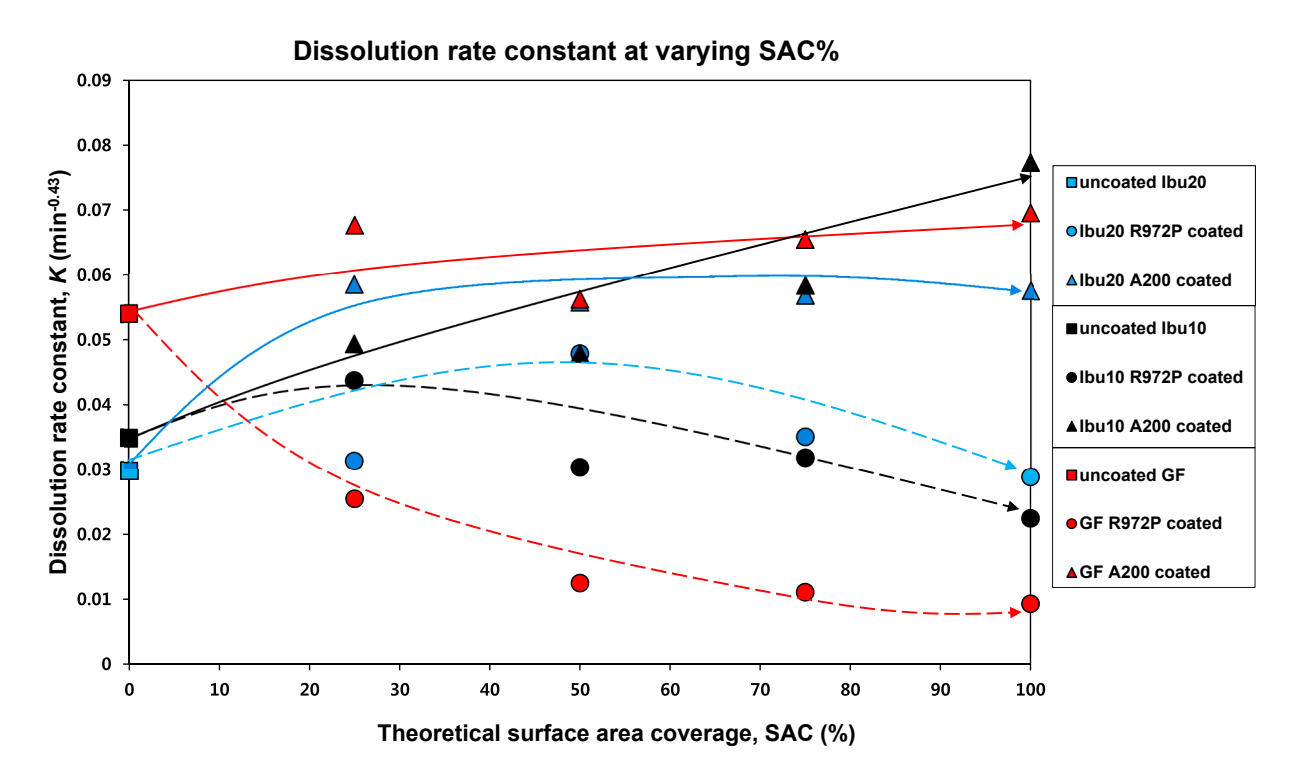


Fig. 7. Dissolution rate constant at varying surface area coverage, SAC%, with the fixed dissolution rate equation exponent (n = 0.43) for ibuprofen20 (Ibu20), ibuprofen10 (Ibu10), and griseofulvin (GF). Trend lines are only illustrative and do not represent a fitted model.

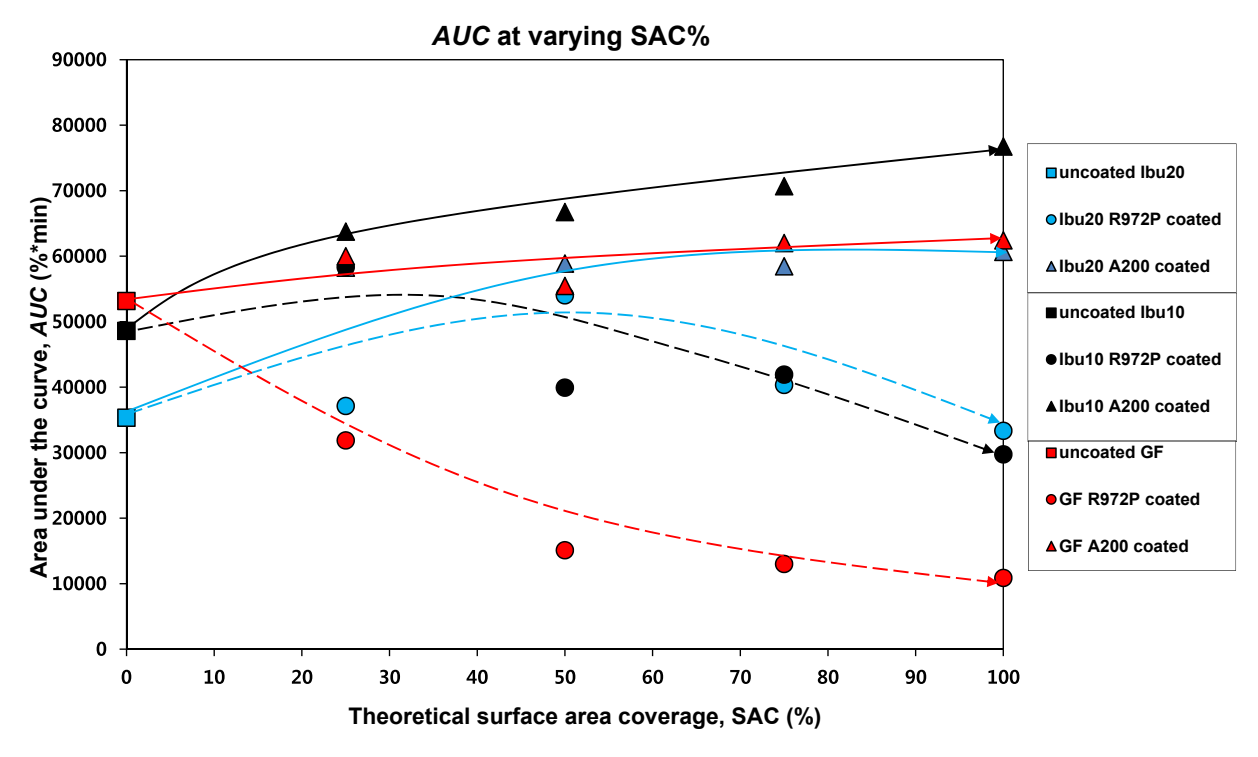


Fig. 8. Area under the dissolution curve (AUC) from 0 to 900 min at varying surface area coverage, SAC% for dry coated ibuprofen20 (Ibu20), dry coated ibuprofen10 (Ibu10), and dry coated griseofulvin (GF). Trend lines are only illustrative and do not represent a fitted model.

For Ibu10, given its smaller size, its highest AUC was observed at R972P 25% SAC, equivalent to 1 wt% silica. While there are no prominent outliers, R972P 50% SAC case appears to be slightly off of the main trend. In that case, the increased surface hydrophobicity may have outweighed the reduced agglomeration effect on its dissolution rate. As was the case for Ibu20, increased SSA effect for Ibu10 well-compensates hydrophobicity effect for at least 25% SAC R972P silica coating, as its AUC is higher than for the uncoated Ibu10 shown as a filled square marker. Likewise, the slopes of the trendlines for A200 and R972P are significantly different.

For GF, Fig. 9(c), while it is similarly sized as Ibu10, the slope of its trendline for R972P is more like Ibu20 that is double its size. It appears that the surface hydrophobicity could be the driver for its dissolution since the reduction in the interparticle cohesion was not as effective as for Ibu10 and Ibu20. That is evident from the filled square marker representing uncoated GF being higher than all R972P coated cases. Interestingly, the slope of the GF trendline for A200 is also more like Ibu20, although not significantly different from that of Ibu10.

Overall, the combined effect of the surface hydrophobicity and agglomerate size appears to be captured by  $\cos\theta/d_{3,2}$  for all three cases although it cannot explain differing behavior of hydrophobic and hydrophilic silica coating. Therefore, advanced modeling and analysis may be required to fully understand the complex behavior of drug powder agglomerate dissolution.

# 4. Conclusions

The investigation of the dissolution behavior of two sizes of ibuprofen and griseofulvin as a function of the type and amount of silica coating indicated that changes in surface hydrophobicity and reduced agglomeration are the main drivers. Dry coating of the ibuprofen particles dramatically reduced their cohesion as evidenced by their FFC values evaluated via shear testing. Further, the agglomerate sizes were reduced by one to two orders of magnitude. When hydrophobic silica R972P was used, such dramatic agglomerate size reduction outweighed the adverse impact of increased surface hydrophobicity for both sizes of

ibuprofen at relatively low levels of surface areas coverage. Perhaps not coincidentally, the amount of hydrophobic silica when that occurred was about the same, 1 wt%, for both ibuprofen sizes, corresponding to 25% SAC for Ibu10 and to 50% SAC for Ibu20. For GF, the other selected drug, cohesion reduction was not as dramatic as for ibuprofen. Hence the reduction in agglomerate size was also much lower and could not overcome the effect of increased drug particle hydrophobicity after coating with hydrophobic silica R972P. Interestingly, the behavior of GF is in line with conventional wisdom that coating with hydrophobic silica is not conducive to improved dissolution. Nonetheless, for many poorly water-soluble drug powders, dry coating with hydrophobic silica would likely be very effective in reducing cohesion. Therefore, even hydrophobic coating could promote their dissolution. For hydrophilic silica, its coating led to both the agglomerate size reduction and reduced surface hydrophobicity. Consequently, the improvement in the dissolution rate appears to be driven by their combined effect. In summary, although the dissolution from drug agglomerates is a complex process, the combined effect of the drug particle surface hydrophobicity and agglomerate size, represented through the external SSA of the agglomerate, could explain the dissolution behavior of micronized particles of poorly water-soluble drugs. Overall, although the current work only utilized LabRAM for dry coating and did not employ industry relevant devices such as comil or fluid energy mill, the outcomes reported are expected to be similar is those devices are used judiciously as discussed in previous work (Deng et al. 2015; Huang et al. 2015a; Chen et al. 2020; Chen et al. 2018b; Mullarney et al. 2011).

#### CRediT authorship contribution statement

**Sangah Kim:** Conceptualization, Methodology, Investigation, Formal analysis, Data curation, Writing - original draft. **Ecevit Bilgili:** Methodology, Validation, Writing - review & editing. **Rajesh N. Davé:** Conceptualization, Supervision, Validation, Project administration, Resources, Writing - review & editing, Funding acquisition.

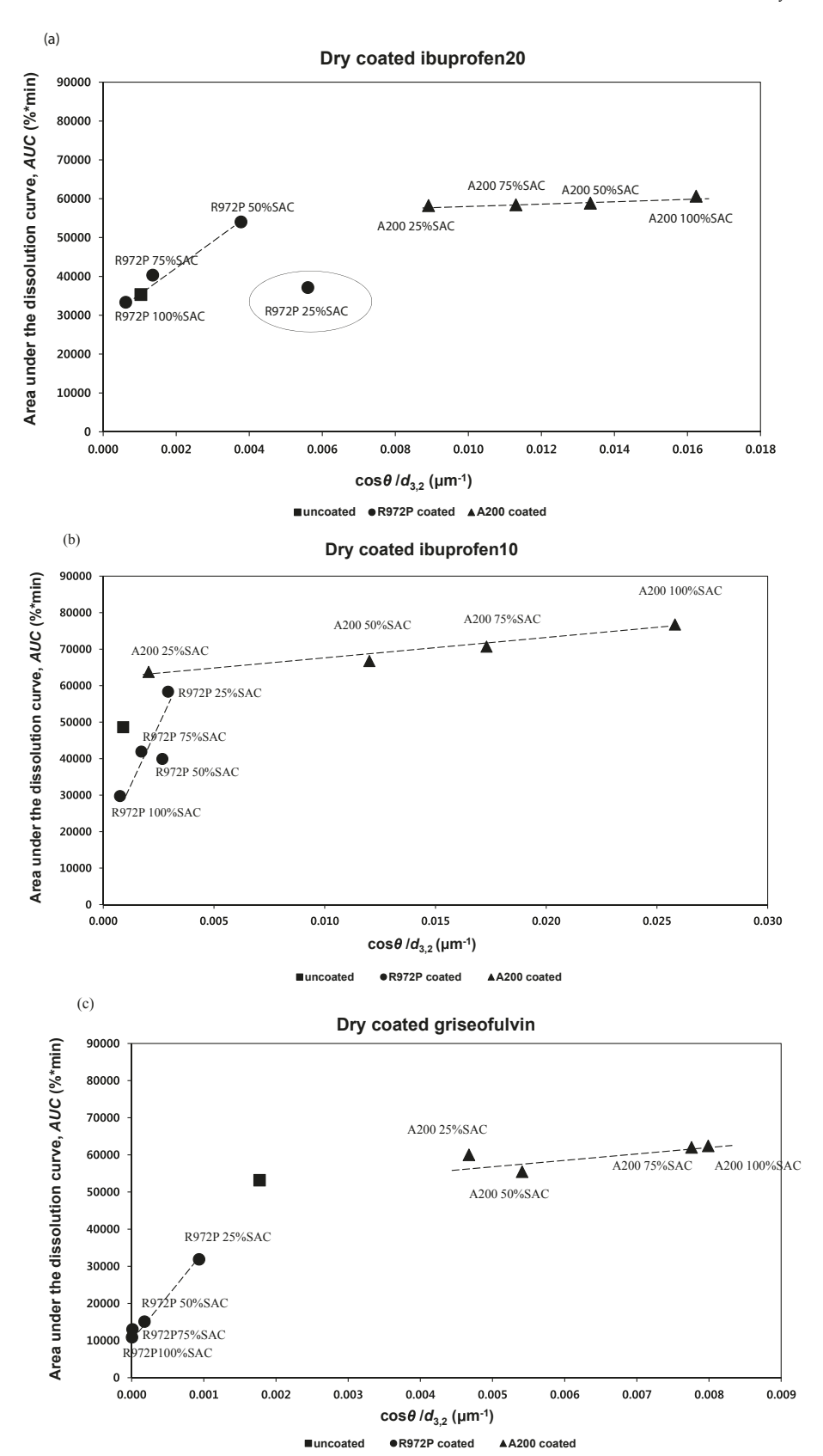


Fig. 9. The area under the dissolution curve (AUC) from 0 to 900 min with respect to the varying ratio between surface wettability to agglomerated particle size ( $\cos\theta/d_{3,2}$ ): For (a) ibuprofen20 (Ibu20); (b) ibuprofen10 (Ibu10); (c) griseofulvin (GF). Uncoated shown in  $\blacksquare$ ; R972P coated drugs shown in  $\blacktriangle$ . Trend lines are only illustrative and do not represent a fitted model.

#### **Declaration of Competing Interest**

The authors declare that they have no known competing financial interests or personal relationships that could have appeared to influence the work reported in this paper.

#### Acknowledgments

The authors are thankful for financial support from National Science Foundation under grant IIP-1919037.

#### Appendix A. Supplementary data

Supplementary data to this article can be found online at https://doi.org/10.1016/j.ijpharm.2021.120853.

#### References

- Alway, B., Sangchantra, R., Stewart, P.J., 1996. Modelling the dissolution of diasepam in lactose interactive mixtures. Int. J. Pharm. 130 (2), 213–224.
- Amidon, G.L., Lennernäs, H., Shah, V.P., Crison, J.R., 1995. A Theoretical Basis for a Biopharmaceutic Drug Classification: The Correlation of in Vitro Drug Product Dissolution and in Vivo Bioavailability. Pharmaceutical Research: An Official Journal of the American Association of Pharmaceutical Scientists 12, 413–420.
- Barra, J., Lescure, F., Falson-Rieg, F., Doelker, E., 1998. Can the organization of a binary mix be predicted from the surface energy, cohesion parameter and particle size of its component? Pharm. Res. 15 (11), 1727–1736.
- Bohin, F., Manas-Zloczower, I., Feke, D.L., 1994. Study of PDMS penetration in silica agglomerates and its influence on dispersion mechanism. Rubber Chemitry and Technology 67 (4), 602–609.
- Bohin, F., Manas-Zloczower, I., Feke, D.L., 1995. Determination of the infiltraion kinetics of polymer into filler agglomerates using transient buoyancy measurements. Powder Technol. 83 (2), 159–162.
- Capece, M., Huang, Z., To, D., Aloia, M., Muchira, C., Davé, R.N., Yu, A.B., 2014.
  Prediction of porosity from particle scale interactions: Surface modification of fine cohesive powders. Powder Technol. 254, 103–113.
- Chander, S., Hogg, R., Fuerstenau, D.W., 2007. Characterization of the wetting and dewetting behavior of powders. Kona Powder Part. J. 25, 56–75.
- Chen, L., He, Z., Kunnath, K.T., Zheng, K., Kim, S., Davé, R.N., 2020. Fine grade engineered microcrystalline cellulose excipients for direct compaction: Assessing suitability of different dry coating processes. Eur. J. Pharm. Sci. 151.
- Chen, L., Ding, X., He, Z., Huang, Z., Kunnath, K.T., Zheng, K., Davé, R.N., 2018a. Surface engineered excipients: I. improved functional properties of fine grade microcrystalline cellulose. Int. J. Pharm. 536, 127–137.
- Chen, L., Ding, X., He, Z., Fan, S., Kunnath, K.T., Zheng, K., Davé, R.N., 2018b. 'Surface engineered excipients: II. Simultaneous milling and dry coating for preparation of fine-grade microcrystalline cellulose with enhanced properties', International Journal of Pharmaceutics 546, 125–136.
- Chen, Y., Yang, J., Davé, R.N., Pfeffer, R., 2008. Fluidization of coated group C powders. AIChE J. 54, 104–121.
- Debacker, A., Makarchuk, S., Lootens, D., Hébraud, P., 2014. Imbibition kinetics of spherical colloidial aggregates. Phys. Rev. Lett. 113 (2).
- de Villiers, M.M., 1996. Influence of agglomeration of cohesive particles on the dissolution behaviour of furosemide powder. Int. J. Pharm. 136, 175–179.
- Deng, X., Scicolone, J., Han, X., Davé, R.N., 2015. Discrete element method simulation of a conical screen mill: A continuous dry coating. Chem. Eng. Sci. 125, 58–74.
- Freeman, R., 2007. Measuring the flow properties of consolidated, conditioned and aerated powders A comparative study using a powder rheometer and a rotational shear cell. Powder Technol. 174, 25–33.
- Forny, L., Marabi, A., Palzer, S., 2011. Wetting, disintegration and dissolution of agglomerated water soluble powders. Powder Technol. 206, 72–78.
- Galet, L., Vu, T.O., Oulahna, D., Fages, J., 2004. The wetting behaviour and dispersion rate of cocoa powder in water. Food Bioprod. Process. 82 (4C), 298–303.
- Garg, N., Pandey, P., Kaushik, D., Dureja, H., 2015. Development of novel multifunction directly compressible co-processed excipient by melt granulation technique. International Journal of Pharmaceutical Investigation 5, 8.
- Ghoroi, C., Han, X., To, D., Jallo, L., Gurumurthy, L., Davé, R.N., 2013. Dispersion of fine and ultrafine powders through surface modification and rapid expansion. Chem. Eng. Sci. 85, 11–24.
- Han, X., Ghoroi, C., Davé, R., 2013a. Dry coating of micronized API powders for improved dissolution of directly compacted tablets with high drug loading. Int. J. Pharm. 442. 74–85.
- Han, X., Jallo, L., To, D., Ghoroi, C., Davé, R., 2013b. Passivation of high-surface-energy sites of milled ibuprofen crystals via dry coating for reduced cohesion and improved flowability. J. Pharm. Sci. 102 (7), 2282–2296.
- Han, X., Ghoroi, C., To, D., Chen, Y., Davé, R.N., 2011. Simultaneous micronization and surface modification for improvement of flow and dissolution of drug particles. Int. J. Pharm. 415, 185–195.
- Huang, Z., Scicolone, J.V., Gurumuthy, L., Davé, R.N., 2015a. Flow and bulk density enhancements of pharmaceutical powders using a conical screen mill: A continuous dry ocating device. Chem. Eng. Sci. 125, 209–224.

- Huang, Z., Scicolone, J.V., Han, X., Davé, R.N., 2015b. Improved blend and tablet properties of fine pharmaceutical powders via dry particle coating. Int. J. Pharm. 478, 447–455.
- Huang, Z., Xiong, W., Kunnath, K., Bhaumik, S., Davé, R.N., 2017. Improving blend content uniformity via dry particle coating of micronized drug powders. Eur. J. Pharm. Sci. 104, 344–355.
- Ji, J., Fitzpatrick, J., Cronin, K., Magurie, P., Zhang, H., Miao, S., 2016. Rehydration behaviour of high protein dairy powders: The influence of agglomeration on wettability, dispersibility and solubility. Food Hydrocolloids 58, 194–203.
- Jallo, L.J., Chen, Y., Bowen, J., Etzler, F., Davé, R.N., 2011. Prediction of inter-particle adhesion froce from surface energy and surface roughness. J. Adhes. Sci. Technol. 25 (4–5), 367–384.
- Jallo, L.J., Ghoroi, C., Gurumurthy, L., Patel, U., Davé, R.N., 2012. Improvement of flow and bulk density of pharmaceutical powders using surface modification. Int. J. Pharm. 423, 213–225.
- Kortejärvi, H., Urtti, A., Yliperttula, M., 2007. Pharmacokinetic simulation of biowaiver criteria: The effects of gastric emptying, dissolution, absorption and elimination rates. Eur. J. Pharm. Sci. 30, 155–166.
- Kunnath, K., Chen, L., Zheng, K., Davé, R.N., 2021. Assessing predictability of packing porosity and bulk density enhancements after dry coating of pharmaceutical powders. Powder Technol. 377, 709–722.
- Kunnath, K., Huang, Z., Chen, L., Zheng, K., Davé, R., 2018. Improved properties of fine active pharmaceutical ingredient powder blends and tablets at high drug loading via dry particle coating. Int. J. Pharm. 543, 288–299.
- Li, M., Ioannidis, N., Gogos, C., Bilgili, E., 2017. A comparative assessment of nanocomposites vs. amorphous solid dispersions prepared via nanoextrusion for drug dissolution enhancement. Eur. J. Pharm. Biopharm. 119, 68–80.

#### Liu, R. 2008. Water-Insoluble Drug Formulation (CRC press).

- Llusa, M., Levin, M., Snee, R.D., Muzzio, F.J., 2010. Measuring the hydrophobicity of lubricated blends of pharmaceutical excipients. Powder Technol. 198, 101–107.
- Mullarney, M.P., Beach, L.E., Dave, R.N., Langdon, B.A., Polizzi, M., Blackwood, D.O., 2011. Applying dry powder coatings to pharmaceutical powders using a comil for improving powder flow and bulk density. Powder Technol. 212, 397–402.
- Naito, M., Hotta, T., Fukui, T., 2003. Applications of Comminution Techniques for the Surface Design of Powder Materials. Key Eng. Mater. 253, 275–292.
- Neirinck, B., Van Deursen, J., Van Der Biest, O., Vleugels, J., 2010. Wettability assessment of submicrometer alumina powder using a modified Washburn method. J. Am. Ceram. Soc. 93, 2515–2518.
- Osorio, J.G., Muzzio, F.J., 2015. Evaluation of resonant acoustic mixing performance. Powder Technol. 278. 46–56.
- Peppas, N.A., 1985. Analysis of Fickian and non-Fickian drug release from polymers. Pharm. Acta Helv. 60, 110–111.
- Pfeffer, R., Dave, R.N., Wei, D., Ramlakhan, M., 2001. Synthesis of engineered particulates with tailored properties using dry particle coating. Powder Technol. 117, 40–67.
- Pingali, K., Mendez, R., Lewis, D., Michniak-Kohn, B., Cuitino, A., Muzzio, F., 2011a. Mixing order of glidant and lubricant - Influence on powder and tablet properties. Int. J. Pharm. 409, 269–277.
- Pingali, K., Mendez, R., Lewis, D., Michniak-Kohn, B., Cuitiño, A., Muzzio, F., 2011b. Evaluation of strain-induced hydrophobicity of pharmaceutical blends and its effect on drug release rate under multiple compression conditions. Drug Dev. Ind. Pharm. 37, 428–435.

# Pubchem. 2005. "National Library of Medicine." In. online: National Center for Biotechnology Information.

- Qu, L., Zhou, Q., Denman, J.A., Stewart, P.J., Hapgood, K.P., Morton, D.A.V., 2015. Influence of coating material on the flowability and dissolution of dry-coated fine ibuprofen powders. Eur. J. Pharm. Sci. 78, 264–272.
- Ritger, P.L., Peppas, N.A., 1987. 'A simple equation for description of solute release I. Fickian and non-fickian release from non-swellable devices in the form of slabs, spheres, cylinders or discs', *Journal of Controlled Release* 5, 23–36.
- Schubert, H., 1993. Instantization of powdered food products. International chemical engineering, 33(1), 28–45.
- Schulze, D., J. Schwedes, and J. W. Carson. 2008. Powders and bulk solids: Behavior, characterization, storage and flow.
- Sievens-Figueroa, L., Pandya, N., Bhakay, A., Keyvan, G., Michniak-Kohn, B., Bilgili, E., Davé, R.N., 2012. Using USP i and USP IV for discriminating dissolution rates of nano- and microparticle-loaded pharmaceutical strip-films. AAPS PharmSciTech 13, 1473–1482.
- Steele, D.F., Moreton, R.C., Staniforth, J.N., Young, P.M., Tobyn, M.J., Edge, S., 2008. Surface energy of microcrystalline cellulose determined by capillary intrusion and inverse gas chromatography. AAPS J. 10, 494–503.
- Swaminathan, V., Cobb, J., Saracovan, I., 2006. Measurement of the surface energy of lubricated pharmaceutical powders by inverse gas chromatography. Int. J. Pharm. 312, 158–165.
- Thakker, M., V. Karde, D. O. Shah, P. Shukla, and C. Ghoroi. 2013. 'Wettability measurement apparatus for porous material using the modified Washburn method', Measurement Science and Technology, 24.
- Washburn, E.W., 1921. The dynamics of capillary flow. Phys. Rev. 17, 273–283.Wu, S., 1973. Polar annd nonpolar interactions in adhesion. The Journal of Adhesion 5 (1), 39–55.
- Yalkowsky, S.H., Banergee, S., 1992. Aqueous solubility: Methods of estimation for organic compounds. New York, NY, Marcek Dekker.
- Yang, J., Sliva, A., Banerjee, A., Dave, R.N., Pfeffer, R., 2005. Dry particle coating for improving the flowability of cohesive powders. Powder Technol. 158, 21–33.

- Yaremko, Z.M., Nikipanchuk, D.M., Fedushinskaya, L.B., Uspenskaya, I.G., 2001. Redispersion of Highly Disperse Powder of Titanium Dioxide in Aqueous Medium. Colloid Journal 63 (2), 253–258.
- Yokoyama, T., Urayama, K., Naito, M., Kato, M., Yokoyama, T., 1987. The Angmill Mechanofusion System and its Applications. Kona Powder Part. J. 5, 59–68.
- Zakhvatayeva, A., Zhong, W., Makroo, H.A., Hare, C., Wu, C.Y., 2018. An experimental study of die filling of pharmaceutical powders using a rotary die filling system. Int. J. Pharm. 553, 84–96.
- Zuo, L., Lourenco, S.D.N., Baudet, B.A., 2019. Experimental insight into the particle morphology changes associated with landslide movement. Landslides 16, 787–798.